AMERICAN JOURNAL OF PHYSICAL ANTHROPOLOGY 101:183–215 (1996)

In Vivo and In Vitro Bone Strain in the Owl Monkey Circumorbital Region and the Function of the Postorbital Septum

CALLUM F. ROSS AND WILLIAM L. HYLANDER
Department of Anatomical Sciences, Health Sciences Center, State University of New York at Stony Brook, Stony Brook, New York 11794-8081 (C.F.R.); Department of Biological Anthropology and Anatomy, Duke University Medical Center, Duke University, Durham, North Carolina 27706 (W.L.H.)

KEY WORDS Anthropoid origins, Lateral orbital wall, Evolutionary morphology, Mastication

ABSTRACT Anthropoids and tarsiers are the only vertebrates possessing a postorbital septum. This septum, formed by the frontal, alisphenoid, and zygomatic bones, separates the orbital contents from the temporal muscles. Three hypotheses suggest that the postorbital septum evolved to resist stresses acting on the skull during mastication or incision. The facial-torsion hypothesis posits that the septum resists twisting of the face about a rostrocaudal axis during unilateral mastication; the transverse-bending hypothesis argues that the septum resists caudally directed forces acting at the lateral orbital margin during mastication or incision; and the tension hypothesis suggests that the septum resists ventrally directed components of masseter muscle force during mastication and incision. This study evaluates these hypotheses using in vitro and in vivo bone strain data recorded from the circumorbital region of owl monkeys.

Incisor loading of an owl monkey skull in vitro bends the face upward in the sagittal plane, compressing the interorbital region rostrocaudally and "buckling" the lateral orbital walls. Unilateral loading of the toothrow in vitro also bends the face in the sagittal plane, compressing the interorbital region rostrocaudally and buckling the working side lateral orbital wall. When the lateral orbital wall is partially cut, so as to reduce the width of its attachment to the braincase, the following changes in circumorbital bone strain patterns occur. During loading of the incisors, lower bone strain magnitudes are recorded in the interorbital region and lateral orbital walls. In contrast, during unilateral loading of the P^3, higher bone strain magnitudes are observed in the interorbital region, and generally lower bone strain magnitudes are observed in the lateral orbital walls. During unilateral loading of the M^2, higher bone strain magnitudes are observed in both the interorbital region and in the lateral orbital wall ipsilateral to the loaded molar.

Comparisons of the in vitro results with data gathered in vivo suggest that, during incision and unilateral mastication, the face is subjected to upward bending in the sagittal plane resulting in rostrocaudal compression of the interorbital region. Modeling the lateral orbital walls as curved plates suggests that during mastication the working side wall is buckled due to the

Received June 14, 1995; accepted May 21, 1996.

Address reprint requests to Callum Ross, Department of Anatomical Sciences, Health Sciences Center, SUNY Stony Brook, Stony Brook, NY 11794–8081.

dorsally directed component of the maxillary bite force which causes upward bending of the face in the sagittal plane. The balancing side lateral orbital wall may also be buckled due to upward bending of the face in the sagittal plane as well as being twisted by the caudoventrally directed components of the superficial masseter muscle force. The in vivo data do not exclude the possibility that the postorbital septum functions to improve the structural integrity of the postorbital bar during mastication. However, there is no reason to believe that a more robust postorbital bar could not also perform this function. Hypotheses stating that the postorbital septum originally evolved to reinforce the skull against routine masticatory loads must explain why, rather than evolving a postorbital septum, the stem anthropoids did not simply enlarge their postorbital bars.

A postorbital septum, formed by contact between the zygomatic and alisphenoid bones, is unique to tarsiers and anthropoids (haplorhines). Its uniqueness, morphological distinctiveness, and proximity to several functional systems in the skull have ensured that the septum has featured prominently in hypotheses of anthropoid relationships as well as in adaptive and functional explanations for anthropoid or haplorhine origins (Cachel, 1979; Cartmill, 1980; Rosenberger, 1986; Ross, 1993, 1995). Several functions for the postorbital septum have been suggested (for reviews see Cartmill, 1980; Rosenberger, 1986; Ross, 1993); among these are three hypotheses suggesting that the postorbital septum functions to resist stresses acting on the skull during mastication or incision. These hypotheses are the facial-torsion hypothesis (Greaves, 1985; Rosenberger, 1986), the transverse-bending hypothesis (Cartmill, 1980), and the tension hypothesis (Rosenberger, 1986).

This study evaluates these three hypotheses using bone strain data recorded from the circumorbital region. In order to do so, it is first necessary to determine the pattern of bone strain that each hypothesis predicts for specific parts of the circumorbital region. This would be fairly simple if, as assumed by Greaves (1985, 1995; Covey and Greaves, 1994), the anthropoid skull can be modeled accurately as a simple structural member (i.e., a beam or cylinder) that is subjected to a specific type of bending or twisting. However, the skull is not a simple structure; it is architecturally complex, and its material properties are anisotropic and heterogeneous. This leads us to suspect that realistic predictions regarding the patterns of strain caused by, for example, twisting the skull about a rostrocaudal axis will be very difficult to make without additional information.

Therefore, an in vitro experiment was designed to determine how the circumorbital region is deformed during twisting or bending of the face on the braincase. This experiment enables us to determine whether the skull behaves as a simple structure when bent and/or twisted as these hypotheses assume and, if it does not, to develop more realistic predictions regarding patterns of in vivo bone strain. Comparison of the in vitro results with bone strain recorded in vivo allows the three hypotheses to be evaluated.

HYPOTHESES

Greaves's facial-torsion hypothesis

Greaves (1985, 1995) hypothesized that during unilateral biting or mastication the mammalian face is twisted relative to the braincase about a rostrocaudal[1] axis because of asymmetrical loading of the skull. This asymmetrical loading is due to the unilateral and vertical components of force acting at the working-side bite point and the balancing-side temporomandibular joint (TMJ). According to Greaves, the upward bite force acting along the left tooth row during mastication or biting on the left side twists the face

[1]See Figure 1B for definition of the terms *rostral, caudal, dorsal,* and *ventral* as applied to the head.

in a counterclockwise direction (in frontal view) about a rostrocaudal axis at the level of the palate (Greaves, 1995), while the reaction force at the right TMJ twists the braincase in a clockwise direction. Greaves argued that twisting of the face on the braincase is most severe in animals that have major components of muscle force acting perpendicular to the long axis of the skull, and he predicts that such animals will have postorbital bars. This includes ungulates, which have large masseter and medial pterygoid muscles, and primates, which have large vertically oriented temporalis muscles.

Greaves also hypothesized that waisting in the orbital region makes this a region of weakness and suggests that the supraorbital torus, postorbital bar, and postorbital septum have evolved as adaptations to counter increased twisting due to this waisting. Moreover, in anthropoids the waisting in the orbital region is accentuated by the extreme approximation of the orbits to the midline, requiring additional support to resist torsional forces acting on the skull: the postorbital septum (Greaves, 1985). Thus, Greaves hypothesizes that the vertical orientation of the enlarged temporalis muscle necessitates the presence of the postorbital bar in primates and approximation of the medial orbital walls to the midline requires the presence of the postorbital septum in anthropoids.

Predictions of Greaves's facial-torsion hypothesis. In analyzing possible torsional moments acting on a skull, only those moments acting to one side of the section under consideration need be analyzed. For example, when predicting patterns of bone strain in the circumorbital region, along section a–a′ in Figure 1, only those moments acting rostral to this section need be analyzed. Following Hylander et al. (1991), we suggest that there are only three torsional moments (torques) acting rostral to the section a–a′ in Figure 1A,B: torques associated with the anterior most fibers of balancing and working side masseters and the torque associated with the bite force. When biting on the left side, the bite force exerts a counterclockwise torque in frontal view, the working (left) side masseter exerts a clockwise torque, and the balancing (right) side masseter exerts a counterclockwise torque (Fig. 1A).

The actual degree of torsion that occurs depends on the relative magnitudes of the torques generated by the bite force and the anterior portions of the two masseters. Our EMG data suggest that in owl monkeys, macaques, and baboons (but not in galagos) the ratios of peak working/balancing side muscle activity approach 1.0 during powerful biting (Hylander, 1979a,b; Hylander et al., in preparation). This suggests that in anthropoids during powerful biting, the torques generated by working and balancing masseters will nearly cancel each other out, leaving the torque imposed at the bite point to twist the face about its rostrocaudal axis.

Interorbital region. The patterns of strain predicted in the interorbital region by Hylander et al. (1991) are shown in Figure 1. If the face is being twisted about a rostrocaudal axis relative to the neurocranium, then the principal strains in the interorbital region are expected to be oriented at approximately 45° to the mid-sagittal plane of the skull (Fig. 1C). The orientations of these principal strains are expected to shift 90° when the chewing side changes.

Lateral orbital wall. If the skull is modeled as a simple cylinder, the following patterns of strain are predicted for the lateral orbital walls. On both the medial and lateral surfaces of the lateral orbital wall, the axis of principal tensile strain is predicted to be oriented upwards and forwards on the chewing or working side and upwards and backwards on the nonchewing or balancing side (Fig. 1A,B). These orientations are predicted to shift 90° when the chewing side changes.

Transverse-bending hypothesis

Cartmill has suggested that the postorbital septum of *Tarsius* supports the postorbital bar "by resisting posteromedially-directed forces produced by tension in the temporalis fascia attached to the lateral orbital margin" (Cartmill, 1980:254). That is, the temporalis muscles pulling backwards (caudally) on the postorbital bars or lateral orbital margins via the temporalis fascia are thought to bend the orbital region in the transverse plane (Cartmill, 1980).

In vivo bone strain data gathered from

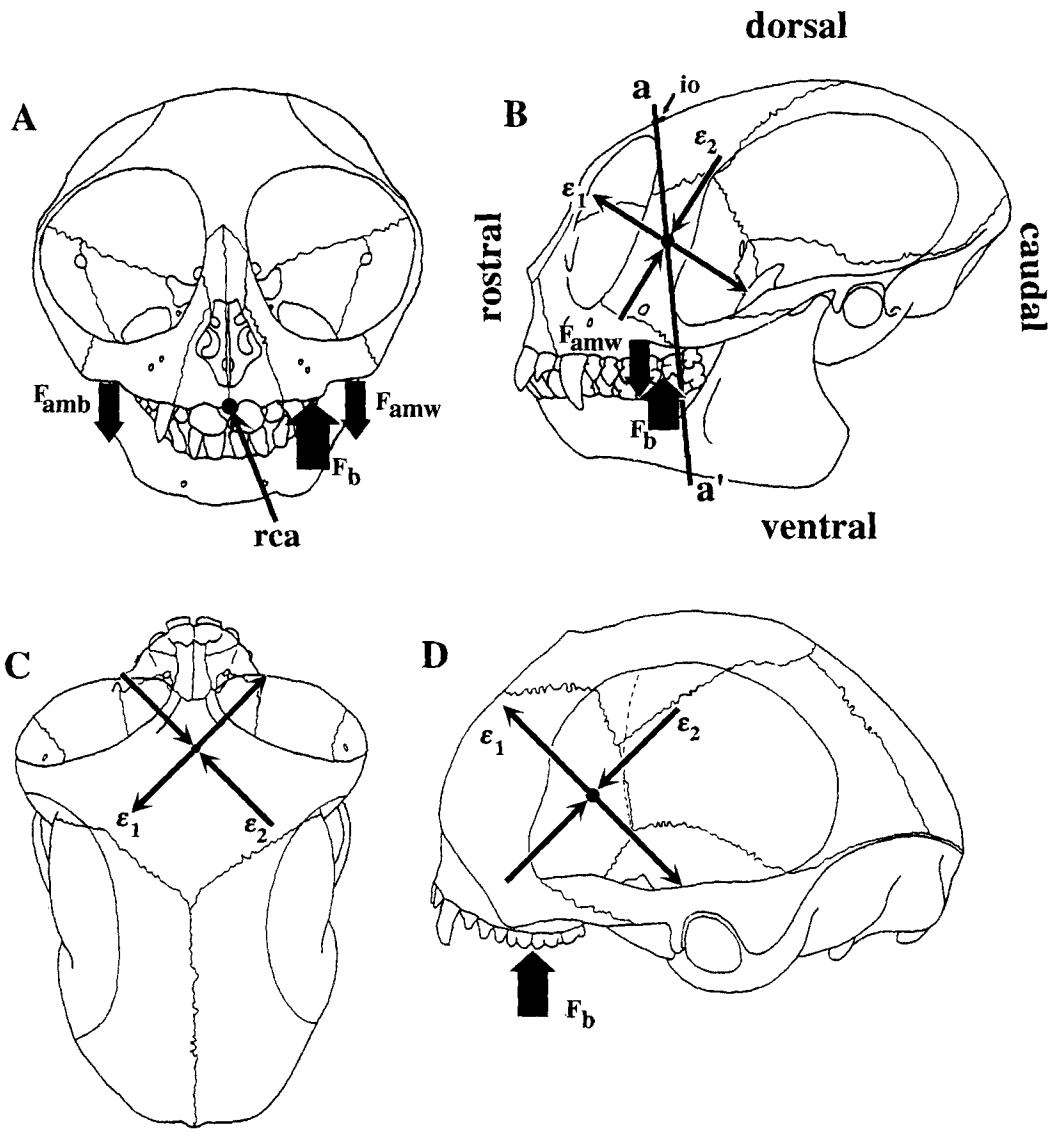

Fig. 1. Diagram illustrating patterns of strain predicted by the facial-torsion hypothesis (Greaves, 1985, 1995; Hylander et al., 1991). In analyzing torsional moments acting on the skull, only those moments acting to one side of the section under consideration (a–a′) need be analyzed, so, when predicting patterns of bone strain in the circumorbital region, only those moments acting rostral to this area need be analyzed. The diagrams illustrate the external forces hypothesized to be acting on the skull rostral to the circumorbital region during mastication and unilateral biting (**A**). The diagrams also illustrate the patterns of strain predicted (**B**) along the lateral surface of the postorbital bar, (**C**) in the interorbital region, and (**D**) on the medial (intraorbital) surface of the postorbital septum. The position of the interorbital gage (interorbital [io]) in lateral view is illustrated in B. The external forces causing torsion of the face on the braincase are the dorsally directed component of the bite force (F_b), the ventrally directed component of the balancing side muscle force (F_{amb}), and the ventrally directed component of the working side masseter muscle force (F_{amw}). When the twisting moments due to F_b and F_{amb} multiplied by their respective moment arms exceed the twisting moment associated with F_{amw} multiplied by its moment arm, the face is predicted to twist about a rostrocaudal axis (rca) positioned at the level of the palate (Greaves, 1995). ϵ_1 = orientation of principal tension; ϵ_2 = orientation of principal compression.

the rostral interorbital region (between the orbits) of macaques suggest that the orbital region may be bent in the transverse plane during mastication (Hylander et al., 1991), a hypothesis further supported by recent recordings from the anterior root of the zygomatic arch (Hylander and Johnson, submitted). Thus, perhaps the lateral orbital margin is pulled backwards during mastication and incision, resulting in transverse bending of the interorbital region. In the context of this loading regime, the postorbital septum can be hypothesized to support the lateral orbital margin against these caudally directed forces (Cartmill, 1980).

Predictions of transverse bending of the face. The complex morphology of the circumorbital region makes it unlikely that this area can be realistically modeled as a set of transversely oriented beams (see also Hylander et al., 1991), and Cartmill's (1980) hypothesis does not model it as such. However, one aim of this study is to determine whether the skull behaves as a simple structure when bent and/or twisted, so the patterns of strain predicted by modeling the circumorbital region as a set of transversely oriented beams are presented here.

Interorbital region. The pattern of strain in the interorbital region depends upon the position of the area to be analyzed relative to the bending plane of neutrality (Fig. 2). In the region lying caudal to the bending plane of neutrality, principal tension is predicted to be parallel to the mid-sagittal plane. In the region lying rostral to the bending plane of neutrality, principal tension is predicted to be oriented perpendicular to the mid-sagittal plane (Fig. 2).

Lateral orbital wall. The postorbital septum is differentiated from the postorbital bar by the temporal line, the septum being that portion of the lateral orbital wall lying caudal to the temporal line and the bar being that portion lying rostral to it. The pattern of strain predicted by this hypothesis varies on either side of the temporal line. If the postorbital bar is modeled as a beam fixed at both ends (Fig. 2), a caudally directed force component would bend the central portion of the beam caudally. In the area in front of the bending plane of neutrality (along the postorbital bar), principal tension is predicted to be oriented rostrocaudally and principal compression oriented dorsoventrally (Fig. 2). Behind the temporal line (along the postorbital septum) the pattern of strain is opposite to that predicted in the postorbital bar (Fig. 2). The backward deflection of the lateral orbital margin is predicted to compress the septum rostrocaudally, resulting in dorsoventrally oriented principal tension.

Rosenberger's tension hypothesis

In addition to twisting of the kind hypothesized by Greaves (1985), Rosenberger (1986:79) also suggests that another loading regime is present, as indicated by the following passage:

> Due to the fused anthropoid symphysis, the contraction of the masseter . . . will produce a large tensile component in the postorbital bar, tending to separate it from the frontal at their suture. By increasing the length of the suture and, more importantly, adding a perpendicular extension that connects the postorbital bar to the sidewall of the skull, increasing the size of the zygomatic bone and giving it mechanical support, the tendency to pull or rotate the lateral pillar out of position is counteracted.

In his Figure 6f (Rosenberger, 1986), reproduced here as Figure 3, Rosenberger appears to suggest that because of the "contraction of masseter" the face is twisted in a clockwise direction (in left lateral view) about a transverse axis passing through the postorbital septa. However, it is impossible for contractions of the masseter to impart a twisting moment such as this because the anterior root of the zygomatic arch (through which the ventrally directed muscle force reaches the septum) lies rostral to the hypothesized axis (see Fig. 3). It is necessary to reformulate Rosenberger's hypothesis in order to determine the patterns of strain that it predicts in the circumorbital region.

Predictions of the tension hypothesis

Interorbital region. The ventrally directed components of force acting on the lateral orbital margins are predicted to pull the lateral edges of the supraorbital region ventrally, resulting in laterally directed tension in the supraorbital region (Fig. 4A).

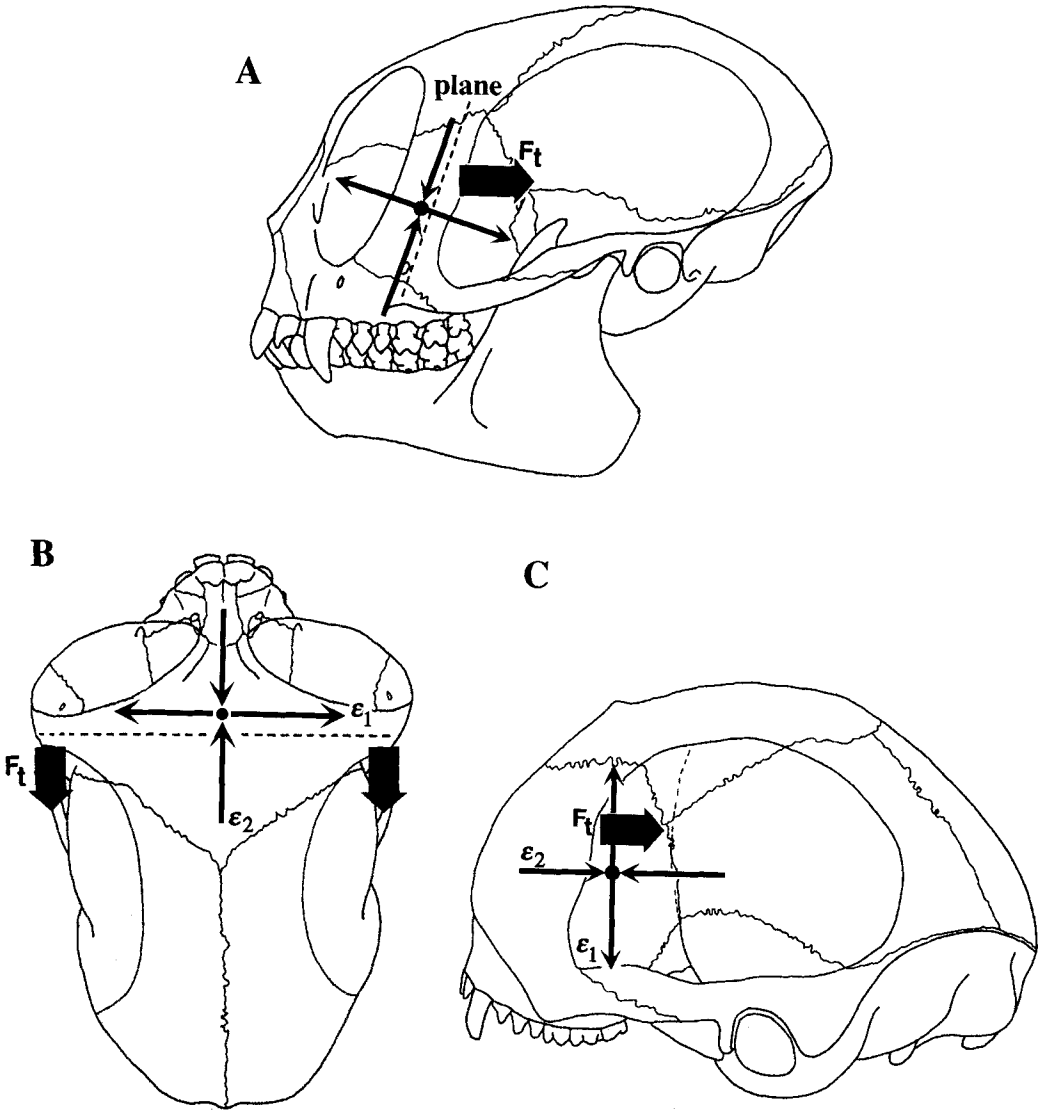

Fig. 2. Diagram illustrating patterns of strain predicted if the upper face (supraorbital region and postorbital bar) is bent caudally in the transverse plane as hypothesized by Cartmill (1980). The external force hypothesized to be causing this bending is the caudally directed component of the temporalis muscle forces acting through the temporalis fascia on each side (F_t). **A:** Illustration of the orientation of the principal strains predicted for the portion of the lateral surface of the postorbital bar lying anterior to the bending plane of neutrality (plane). **B:** Illustration of the orientation of the principal strains predicted for the portion of the interorbital region lying anterior to the bending axis of neutrality (plane). **C:** Illustration of the orientation of the principal strains predicted for the medial surface of the postorbital septum, assuming that the septum lies posterior to the bending plane of neutrality. ϵ_1 = orientation of principal tension; ϵ_2 = orientation of principal compression.

Fig. 3. Rosenberger's (1986) Figure 6f redrawn illustrating the loading regime posited by him to be caused by the inferior component of the masseter muscle force. The pattern of stresses indicated in this figure is impossible if the axis is located as indicated.

Lateral orbital wall—medial and lateral surfaces. The lateral orbital wall can be modeled as a curved plate anchored at the top and posterior edge (Fig. 5A,B). The ventrally directed component of masseter muscle force—hypothesized by Rosenberger (1986) to be important—will load the lateral orbital wall in dorsoventrally oriented tension. The tensile loading regime will tend to "unbend"[2] the lateral orbital wall producing the principal tensile strain orientations illustrated to the left of the dashed lines in Figure 5A. Because the posterior edge of the lateral orbital wall is anchored to the braincase, this unbending will result in shearing forces in the wall producing the principal tensile strain orientations illustrated to the right of the dashed line in Figure 5A. The combination of these two loading regimes (unbending and shear) is predicted to produce principal tensile strain orientations intermediate between the two. Because we have no way of determining which of these loading regimes is more important, the strain orientations predicted for this loading regime will fall within the range of these two values (Fig. 5B). The predicted range of principal tensile strain orientations is shown on the skulls in Figure 4B,C.

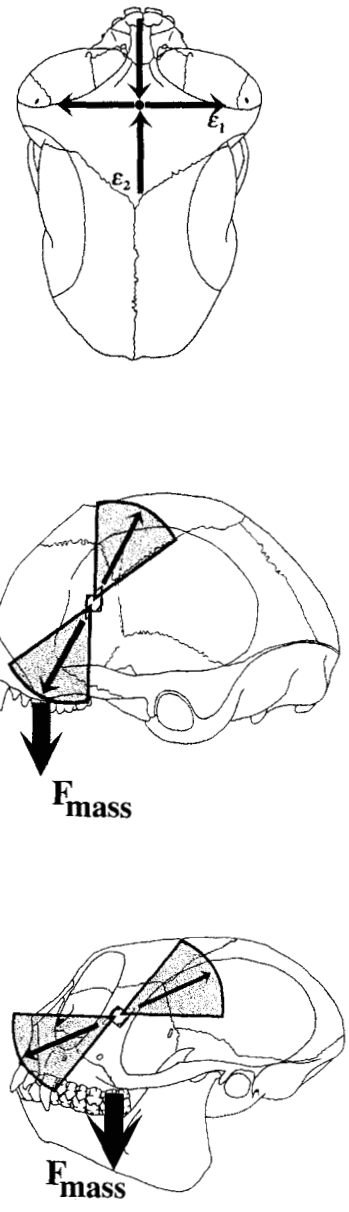

Fig. 4. Diagram illustrating patterns of strain predicted if the most important loading regime in the circumorbital region is ventrally directed tension acting on the lateral orbital wall due to contractions of masseter (F_{mass}), as hypothesized by Rosenberger (1986). The predicted patterns of strain assume that the lateral orbital wall can be modeled as a curved plate fixed dorsally and caudally (see Fig. 5). **A:** Illustration of the orientation of ϵ_1 and ϵ_2 predicted in the interorbital region. **B:** Illustration of the possible range of ϵ_1 orientations predicted along the lateral surface of the lateral orbital wall. **C:** Illustration of the range of ϵ_1 orientations predicted along the medial surface of the lateral orbital wall. ϵ_1 = orientation of principal tension; ϵ_2 = orientation of principal compression.

[2]The term *unbending* is used to refer to bending of a curved plate that pulls the ends further apart, decreasing its curvature, whereas *buckling* refers to bending of a curved plate that pushes the ends closer together, increasing its curvature. The term *buckling* is used solely for its heuristic value and is not meant to imply failure of the kind denoted by the term *Euler buckling*.

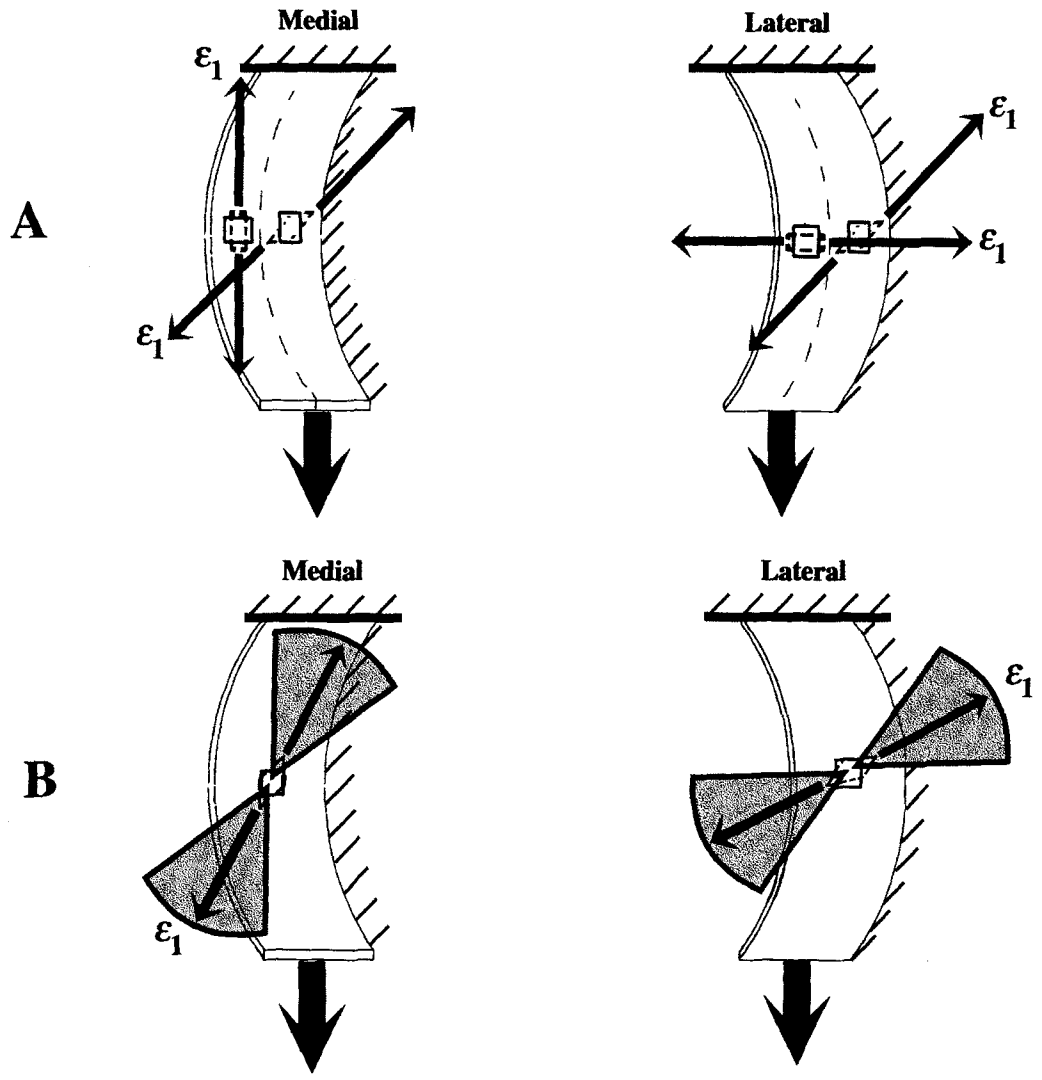

Fig. 5. If the lateral orbital wall can be modeled as a curved plate anchored at the top and posterior edge, the ventrally directed component of masseter muscle force (large arrow) will load the lateral orbital wall in dorsoventrally oriented tension. The tensile loading regime will tend to unbend the lateral orbital wall producing the ϵ_1 orientations illustrated to the left of the dotted lines in **A.** Because the posterior edge of the lateral orbital wall is anchored to the braincase, this unbending will result in shearing forces in the wall producing the principal tensile strain orientations illustrated to the right of the dotted line in A. The combination of these two loading regimes (unbending and shear) is predicted to produce principal tensile strain orientations intermediate between the two. At present we do not know which of these loading regimes is more important, so the strain orientations predicted for this loading regime might range between the two extremes **(B).** These principal tensile strain orientations are shown on the skulls in Fig. 4B,C.

Testing the three hypotheses

These three hypotheses predict mutually exclusive combinations of strain orientations in the postorbital bar, postorbital septum, and interorbital region of anthropoids. These predictions enable us to determine which of these loading regimes is most likely to be important during mastication and incision. The absence of the pattern of strain predicted by each model serves to falsify the

hypothesis that the postulated loading regime is the most important one acting on the skull—and suggests that the bones of that region are not adapted to withstand the hypothesized loads. However, the converse is not true; that is, if the pattern of strain is as predicted by a particular model, this does not necessarily imply that the postorbital septum functions to reduce levels of stress and strain associated with this loading regime (cf. Hylander et al., 1991). To assume this presupposes that the postorbital septum does indeed function to provide structural integrity for the anthropoid circumorbital region, which is the point in question. This question is better rephrased: In the absence of the postorbital septum, can the circumorbital region of anthropoids effectively counter loads associated with mastication and biting? Two approaches are taken to answering this question.

First, high levels of in vivo bone strain in these regions are taken to indicate that the absence of the postorbital septum might result in a serious structural deficiency for the circumorbital region. In macaques, the highest bone strain magnitudes recorded so far in the skull in vivo are found in the mandibular corpus (Hylander et al, 1991, unpublished data). Similarly for this study, bone strain magnitudes in the circumorbital region are determined to be high if they are similar to or higher than those recorded from the corpus of the mandible.

The second approach involves in vitro analysis of bone strain levels in the circumorbital region in a skull with and without a postorbital septum. The skull is loaded artificially in various ways (e.g., facial torsion, incisor loading), and strains in the circumorbital region are measured. The structural capabilities of the septum are then eliminated by cutting it, and the skull is loaded again in an identical manner. If strain levels in the skull without the support of the septum are higher than those in the skull with the septum, then the septum can be claimed to provide additional strength to the circumorbital region. However, if there is no significant increase in strain magnitudes following removal of the septum, its presence cannot be claimed to be a significant contribution to the structural integrity in this region. As it is presently impossible to load a skull in vitro in such a way as to replicate the precise in vivo situation, the in vitro experiment was designed to determine whether strain magnitudes associated with simple loading regimes (i.e., a single load applied at different points along the tooth row) are higher when the structural capabilities of the postorbital septum are absent.

MATERIALS AND METHODS

In vitro experiment

Specimen and preparation. The cadaver of a single subadult owl monkey (canines half erupted) was obtained from the Smithsonian Institution. The specimen had been preserved in 30% alcohol for an unknown period of time. The head was removed from the body, and the eyes, skin, masticatory muscles, connective tissue and periosteum were removed from the skull. The soft palate and parts of the medial pterygoid muscle were left in place. The brain was largely removed.

The back of the skull was embedded in epoxy (Caroplastic; Carolina Biological Supply Co., Burlington, NC) so that the epoxy flowed through the foramen magnum into the occipital part of the braincase. The posterior roots of the zygomatic arches were not embedded in the epoxy. Care was taken to ensure that the bone remained wet at all times during preparation and during the experiment.

Strain gage placement. Three delta-stacked rosettes (SA-06-030WY-120; Micro-measurements, Raleigh, NC) were bonded to the skull: one on the midline in the interorbital region, 7–8 mm caudal to nasion, one on the lateral surface of the left postorbital bar (i.e., anterior to the temporal line) midway between the anterior root of the zygoma and the junction of the postorbital septum and the braincase, and one on the medial surface of the left postorbital bar, just below the level of the gage on the lateral surface. A small area of the cortical bone was degreased (chloroform and methanol) and neutralized (M-Prep Neutralizer 5A (ammonia water); Measurement Group Inc., Raleigh, NC) and then the rosette bonded to it with a cyanoacrylate adhesive. Radiographs were taken

in dorsoventral and mediolateral perspectives to document the orientations of the rosette elements.

Recording procedure. The delta rosette strain gages were connected so that each element of the strain gage formed one arm of a Wheatstone Bridge. Bridge excitation was 1 volt. Voltage changes were conditioned and amplified on a Vishay 2100 system and then recorded on 1 inch magnetic tape of a 14-channel FM tape recorder at 15 inches/second.

Technique for applying loads to the skull. The skull was secured upside down by fixing the epoxy block into a bench vise, and a series of loads was applied to various points along the tooth row. To ensure that the skull could be oriented in the same way relative to the gravity vector before and after cutting the septa, the tooth row was oriented horizontally using a spirit level. The loads applied to the skull consisted of lead sinkers attached via snap swivels and nylon fishing line to #1 fishhooks. The tips of the fishhooks were placed at five points along the toothrow and strains recorded. Loads were applied sequentially between the I^1s and in the talon basins of the left and right P^3s and M^2s.

The postorbital septa on both sides were then cut using a dental drill. The cuts extended from the inferior orbital fissure at the zygomatico-alisphenoid suture to the temporal line slightly superior to the zygomatico-frontal suture (Fig. 6). The minimum distance from the cut to the superior orbital margin was 3.5 mm on each side. The skull was placed under the five loading regimes defined above while strains were recorded. The load applied was 733.2 g at each of the five points on the tooth row. Each loading regime was repeated ten times before and after cutting the septa.

Analysis of strain data. The strain data were played out from the tape recorder and onto a chart at a tape speed of 1-7/8 inches/second and a chart recorder speed of 5 mm/second. The peak strains were calculated by reading the strain values directly from the chart recording. They were then entered in a PC microcomputer, and the direction and magnitude of the maximum and minimum principal strains and the magnitude of the shear strains were calculated following the equations in Dally and Riley (1965).

Strain (ϵ), a dimensionless unit equaling the change in length of an object divided by its original length, is measured in microstrain ($\mu\epsilon$) units which are equal to 1×10^{-6} inches/inch or mm/mm. Tensile strain is registered as a positive value and compressive strain as a negative value. The maximum principal strain (ϵ_1) is usually the largest tensile strain value, while the minimum principal strain is usually the largest compressive strain value (ϵ_2). ϵ_1 minus ϵ_2 is equal to the maximum shear strain, or γ-max.

For each loading regime before and after cutting the septa, descriptive statistics were calculated for the magnitude of ϵ_1, ϵ_2, the ratio ϵ_1/ϵ_2, and γ-max and for the orientation of ϵ_1 (ϵ_2 is oriented at 90° to ϵ_1.) Unpaired one-tailed t-tests (P) < 0.05) were used to determine whether those values recorded after cutting the postorbital septa were different from those recorded before.

In vivo experiment

Subjects. Two adult owl monkeys (*Aotus* sp.), one male and one female, served as subjects. These two animals were chosen because they had previously experienced unilateral enucleation (i.e., had the orbital contents removed) for reasons unrelated to our research. This enabled placement of a strain gage on the medial surface of the postorbital septum. Enucleation occurred several years before our research on the animals, when the animals were adults. No skeletal asymmetries were apparent from measures of orbit diameter based on external landmarks or radiographs.

Strain-gage placement. During seven different experiments, strain gages were placed in various combinations 1) along the interorbital region (roughly corresponding to the dorsal interorbital region of Hylander et al. [1991]) 2) on the lateral surface of the postorbital bar, 3) on the medial surface of the postorbital septum, and 4) on the lateral surface of the mandibular corpus below the M_1 (Table 1). The animals were food-deprived for 24 hours before each experiment

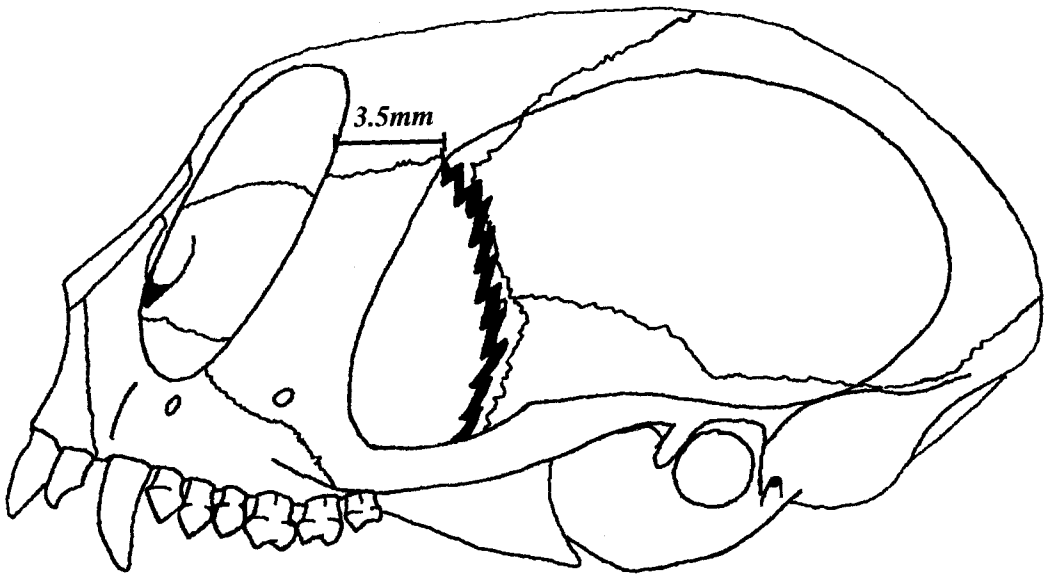

Fig. 6. Diagram illustrating position of cut in postorbital septa during in vitro experiment. The cut was bilateral (i.e., both septa were cut). The shortest distance from the top of the cut to the orbital margin is 3.5 mm.

and heavily sedated using an intramuscular injection of ketamine and acepromazine (Connolly and Quimby, 1978). A local anesthetic (2% Lidocaine HCl with epinephrine 1:100,000) was infiltrated subcutaneously over the area where the strain gage was to be bonded. As well as eliminating discomfort to the animal, the local anesthetic also provided adequate hemostasis. About 5 min after infiltration a small incision was made, the skin overlying the gage site was reflected, and the periosteum was elevated to expose the bone. The bone was degreased and neutralized and the delta rosette bonded to the bone as described above for the in vitro experiment. Following bonding of the strain gage, the incision was closed with sutures, with the lead wires of the strain gage passing out through the wound. Dorsoventral and lateral radiographs were taken to document strain gage position and orientation.

Recording procedure. The animals were then placed in a monkey sling-suit (a modified cat-restraint suit) made to our specifications by Alice King Medical Arts (Hawthorne CA) Each of the three elements of the rosettes was connected to form one arm of a Wheatstone Bridge. The animals were presented hard apricots, hard prunes, prune stones, and gelatin candies ("gummy bears"). Strains were recorded while the animals incised and chewed these foods. The subject's behavior (e.g., incision, molar bite, mastication) and chewing side were recorded on the voice track of the tape recorder.

TABLE 1. Strain gage placement and owl monkeys used in in vivo experiments

Experiment	Owl monkey	Strain gage placement
4	1	Left postorbital septum
6	2	Left postorbital septum
7	1	Right postorbital bar Interorbital region
8	2	Right postorbital bar Interorbital region
9	2	Left postorbital bar Left mandibular corpus
10	1	Left postorbital bar Left mandibular corpus
13	1	Interorbital region

Strain analysis. Strain analysis proceeded as for the in vitro study. Descriptive

statistics were calculated for the magnitude of ϵ_1, ϵ_2, the ratio of ϵ_1/ϵ_2, γ-max, and the orientation of ϵ_1 recorded during mastication and incision of each food type. Within each region (i.e., interorbital, postorbital bar, postorbital septum) mean orientations of ϵ_1 recorded during incision, chewing on the left and chewing on the right, were compared with each other using unpaired two-tailed *t*-tests.

IN VITRO RESULTS

The results of the in vitro experiment are presented and discussed first to aid in interpreting the patterns of in vivo bone strain. The mean values of γ-max, ϵ_1 and ϵ_2, the ratio of ϵ_1/ϵ_2, and the mean orientation of ϵ_1 recorded in the in vitro experiment are presented in Tables 2–6. Figures 7–9 illustrate the mean orientations of the principal tensile strain in the interorbital region (Fig. 7) and on the lateral (Fig. 8) and medial (Fig. 9) surfaces of the lateral orbital wall before and after cutting both septa.

In the first part of this discussion, the observed patterns of strain orientation recorded under each of the different loading conditions are related to the external loads that were applied. Patterns of strain recorded before and after cutting the septa are compared. In the second part of this discussion, the changes in strain magnitude caused by cutting the septa are used to suggest the possible role that the postorbital septum plays in redistributing or reducing strain in the skull. In this experiment, strain gages were placed on the left lateral orbital wall, so in discussing the in vitro experiment, the term *working side* refers to the left side of the skull when the left tooth row was loaded and *balancing side* refers to the left side of the skull when the right tooth row was loaded.

Strain orientations

Incisor loading

Before cutting the septa. Loading the incisors generates, in the interorbital region, tension directed perpendicular to the mid-sagittal plane (Fig. 7), on the lateral surface of the postorbital bar, dorsoventrally oriented tension (Fig. 8), and, on the medial surface of the postorbital bar, tension oriented caudally and dorsally at approximately 45° to the tooth row (Fig. 9).

After cutting the septa. Cutting the postorbital septa resulted in only minor changes in the orientation of ϵ_1 recorded from the interorbital region (Fig. 7) and lateral surface of the postorbital bar (Fig. 8). On the medial surface of the bar, there was a 25° counterclockwise shift in the orientation of ϵ_1, bringing it close to orthogonal to the orientation of ϵ_1 on the lateral surface (Fig. 9; Table 6).

Loading of the P^3 and M^2

Before cutting the septa. ϵ_1 orientations recorded from the interorbital region during unilateral loading of P^3 and M^2 are similar to those observed during incisor loading (i.e., almost directly lateral) (Fig. 7). ϵ_1 orientations recorded from the medial (Fig. 9) and lateral (Fig. 8) surfaces of the working side postorbital bar are nearly orthogonal to each other, those on the lateral surface being slightly clockwise of dorsoventral and those on the medial surface being slightly clockwise of rostrocaudal. ϵ_1 orientations on the lateral surface of the balancing side postorbital bar (Fig. 8) are more dorsoventrally directed than those on the working side, whereas ϵ_1 orientations on the medial surface during P^3 loading (Fig. 9) are dorsal and rostral at approximately 45° to the plane of the tooth row. It was not possible to analyze the data gathered from the medial surface of the balancing side postorbital bar because electrical interference distorted the signal during recording.

After cutting the septa. After cutting the postorbital septa, ϵ_1 in the interorbital region is oriented slightly counterclockwise of perpendicular to the mid-sagittal plane during loading of the right P^3 and M^2 but slightly clockwise of perpendicular to the mid-sagittal plane during loading of the left P^3 and M^2. ϵ_1 orientations recorded from medial (Fig. 9; Table 6) and lateral (Fig. 8) surfaces of the working side postorbital bar during P^3 loading are largely unaffected by cutting the septa. In contrast, ϵ_1 orientations recorded from medial (Fig. 9) and lateral (Fig. 8) surfaces of the working side postorbital bar during M^2 loading are rotated

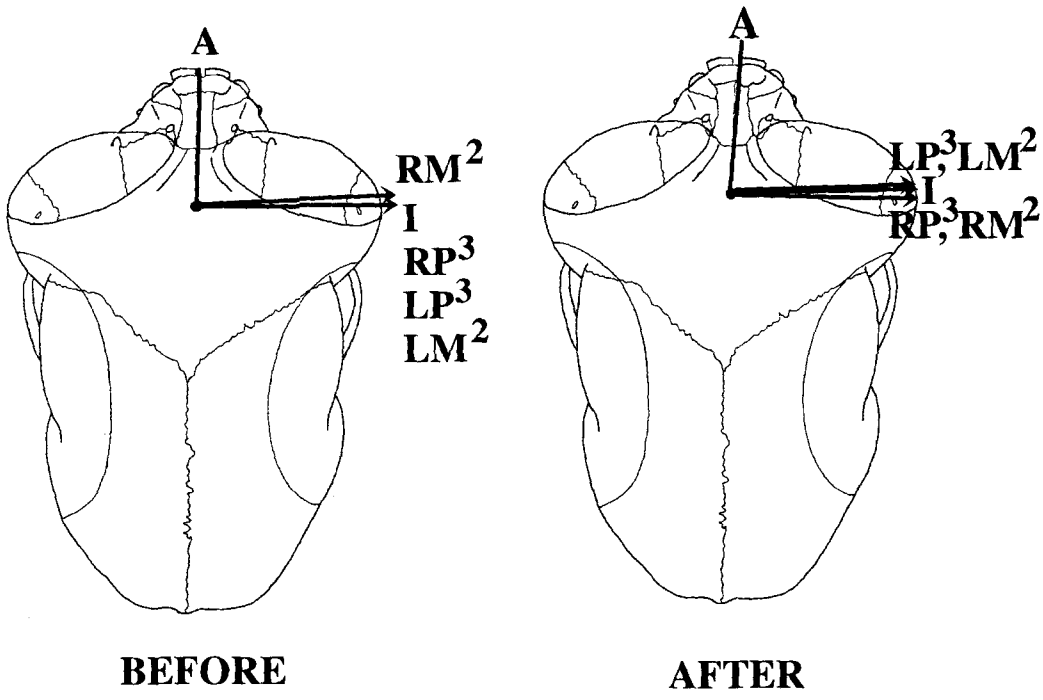

Fig. 7. Orientation of ϵ_1 in the interorbital region before and after cutting the postorbital septa. A, orientation of A-element. Shown are the orientations of ϵ_1 (principal tension) during loading of incisors (I), left molar (LM^2), left premolar (LP^3), right molar (RM^2), right premolar (RP^3).

slightly clockwise after the septa were cut, but they are still almost orthogonal to one another. ϵ_1 orientations recorded from the lateral (Fig. 8) surface of the balancing side postorbital bar during P^3 loading are rotated counterclockwise by 64°, and ϵ_1 orientations on the medial surface are rotated 71° clockwise, bringing ϵ_1 orientations on the medial and lateral surfaces of the balancing side lateral orbital wall almost orthogonal to each other (Table 6). This change is accompanied by a change in the ϵ_1/ϵ_2 ratio on the lateral surface from predominantly tensile (i.e., >1.00) to predominantly compressive (i.e., <1.00) and the change in this ratio on the medial surface from predominantly compressive to predominantly tensile (Table 5). ϵ_1 orientations recorded from the lateral (Fig. 8) surface of the balancing side postorbital bar during M^2 loading are predominantly rostrocaudal; ϵ_1 orientations recorded from the medial surface are rostral and dorsal at approximately 45° to the tooth row.

Strain magnitudes

Incisor loading. Under conditions of incisor loading, bilateral cuts in the postorbital septa cause a slight decrease in γ-max and ϵ_1 magnitudes in the interorbital region and large decreases in γ-max, ϵ_1, and ϵ_2 magnitudes along the medial and lateral surfaces of the postorbital bar (Tables 2–4).

Loading P^3. Under conditions of unilateral loading of the P^3, cutting the septa causes slight increases in the magnitude of γ-max in the interorbital region and significant decreases in the magnitudes of γ-max recorded from both surfaces of the balancing side postorbital bar (Table 2). The ratio of ϵ_1/ϵ_2 recorded from the lateral surface of the balancing side postorbital bar changes from predominantly tensile to predominantly compressive (Table 5) due to increases in ϵ_2 magnitudes and decreases in ϵ_1 magnitudes (Tables 3, 4). In contrast, on the medial surface the ratio of ϵ_1/ϵ_2 changes from predomi-

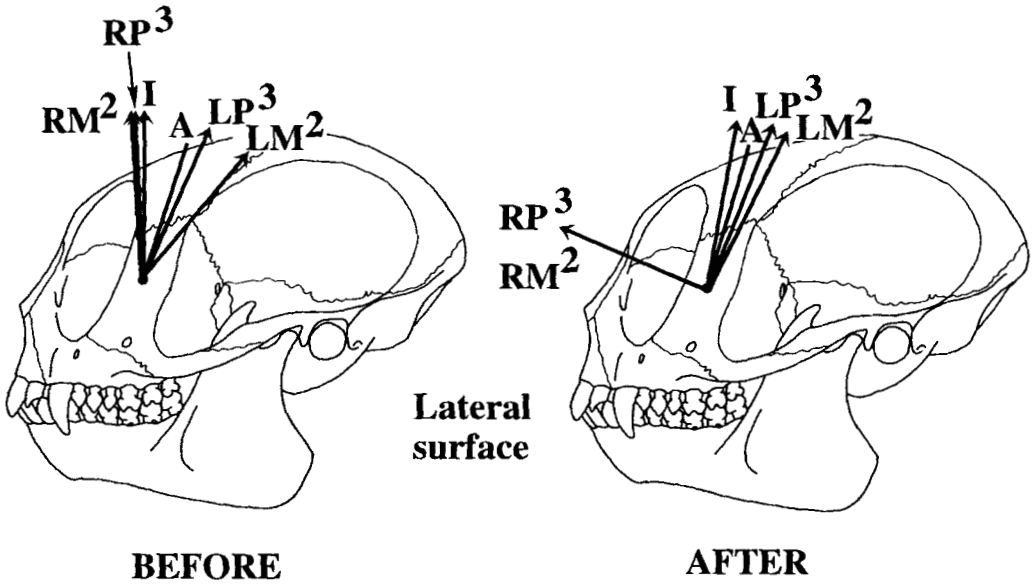

Fig. 8. Orientation of ϵ_1 along the lateral surface of the postorbital bar before and after cutting the postorbital septa. A, orientation of A-element. Shown are the orientations of ϵ_1 (principal tension) during loading of incisors (I), left molar (LM^2), left premolar (LP^3), right molar (RM^2), right premolar (RP^3).

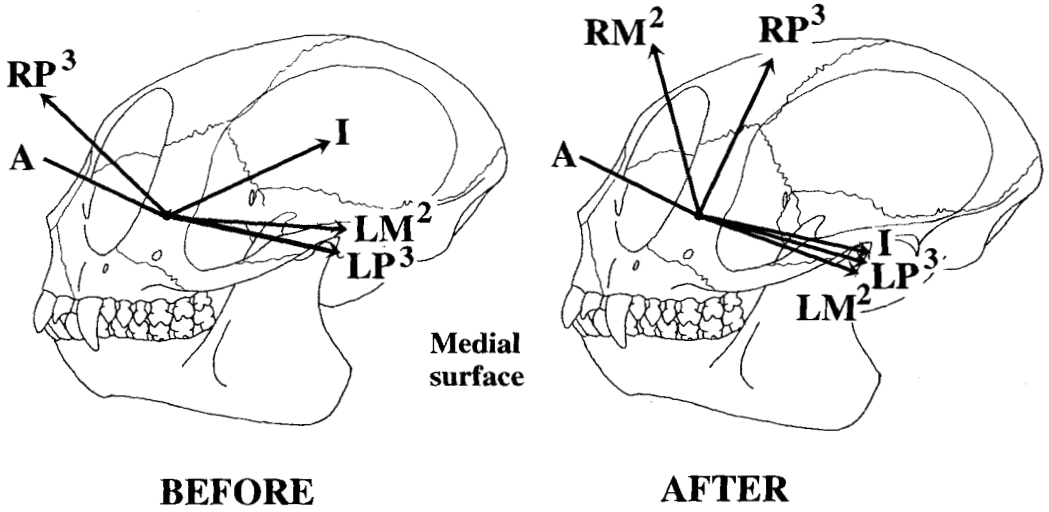

Fig. 9. Orientation of ϵ_1 along the medial surface of the postorbital bar before and after cutting the postorbital septa. A, orientation of A-element. Shown are the orientations of ϵ_1 (principal tension) during loading of incisors (I), left molar (LM^2), left premolar (LP^3), right molar (RM^2), right premolar (RP^3).

nantly compressive to predominantly tensile (Table 5) due to decreases in ϵ_2 magnitudes (Table 4). No significant changes in γ-max are observed on the lateral surface of the working side postorbital bar, but a marked decrease in γ-max is recorded on the medial surface (Table 2). Along the working side bar, tensile strains remain highest on the lateral

TABLE 2. Mean (and standard deviation) γ-max (in microstrain units) recorded in vitro from the interorbital region and lateral and medial surfaces of the left postorbital bar before (B) and after (A) cutting postorbital septa (n = 10 loadings before and after)[1]

	I	Right P^3	Right M^2	Left P^3	Left M^2
Interorbital region					
B	190 (7.3)	129 (8.6)	90 (8.7)	120 (4.0)	74 (2.4)
A	181 (3.6)	132 (3.7)	115 (6.3)	134 (5.5)	115 (2.2)
%*	−5	+2	+28	+12	+55
Postorbital bar (lateral)					
B	118 (4.2)	44 (2.5)	34 (3.4)	150 (9.1)	122 (4.1)
A	49 (1.6)	32 (2.9)	36 (5.6)	147 (6.0)	171 (2.9)
%	−58	−27	ns	ns	+40
Postorbital bar (medial)					
B	111 (10.9)	40 (3.7)	—	138 (9.5)	103 (4.6)
A	34 (3.5)	28 (3.7)	29 (2.4)	108 (4.5)	109 (6.6)
%	−69	−30		−22	+6

[1]Loading regimes: I, incisor loading; right P^3 and right M^2, unilateral loading of right P^3 and right M^2; left P^3 and left M^2, unilateral loading of left P^3 and M^2.
*% = statistically significant ($P < 0.05$) changes in γ-max caused by cutting the septa expressed as a percentage of γ-max before the septa were cut. ns = no significant difference between the values recorded before and after cutting the septa.

TABLE 3. Mean (and standard deviation) ϵ_1 magnitude (in microstrain units) recorded in vitro from the interorbital region and lateral and medial surfaces of the left postorbital bar before (B) and after (A) cutting postorbital septa (n = 10 loadings before and after)[1]

	I	Right P^3	Right M^2	Left P^3	Left M^2
Interorbital region					
B	90 (2.7)	72 (1.4)	62 (3.9)	59 (3.1)	46 (1.3)
A	88 (1.5)	74 (1.4)	72 (3.2)	68 (2.6)	62 (1.7)
%*	−2	ns	+16	+15	+35
Postorbital bar (lateral)					
B	73 (2.7)	27 (2.2)	21 (1.4)	103 (4.2)	82 (2.9)
A	33 (1.2)	11 (0.8)	12 (1.4)	107 (4.2)	115 (2.2)
%	−55	−59	−43	ns	+40
Postorbital bar (medial)					
B	49 (8.7)	17 (2.2)	—	52 (4.2)	38 (1.8)
A	12 (1.6)	17 (1.6)	18 (1.8)	41 (1.8)	42 (3.6)
%	−76	ns		−21	+10

[1]Loading regimes: I, incisor loading; right P^3 and right M^2, unilateral loading of right P^3 and right M^2; left P^3 and left M^2, unilateral loading of left P^3 and M^2.
*% = statistically significant ($P < 0.05$) changes in ϵ_1 magnitude caused by cutting the septa expressed as a percentage of ϵ_1 magnitude before the septa were cut. ns = no significant difference between the values recorded before and after cutting the septa.

TABLE 4. Mean (and standard deviation) ϵ_2 magnitude (in microstrain units) recorded in vitro from the interorbital region and lateral and medial surfaces of the left postorbital bar before (B) and after (A) cutting postorbital septa (n = 10 loadings before and after)[1]

	I	Right P^3	Right M^2	Left P^3	Left M^2
Interorbital region					
B	−100 (4.7)	−57.4 (4.8)	−28 (5.5)	−60 (1.3)	−28 (2.0)
A	−93 (2.2)	−57.7 (2.6)	−43 (3.6)	−66 (3.3)	−53 (0.5)
%*	ns	ns	+54	+10	+89
Postorbital bar (lateral)					
B	−45 (2.5)	−16 (1.4)	−24 (1.8)	−47 (3.3)	−39 (1.4)
A	−17 (0.6)	−21 (2.3)	−13 (4.3)	−41 (2.3)	−56 (1.7)
%	−62	+31	−46	−13	+44
Postorbital bar (medial)					
B	−62 (2.9)	−23 (1.9)		−86 (6.0)	−65 (3.2)
A	−22 (2.3)	−12 (3.2)	−11 (0.9)	−67 (3.2)	−67 (4.0)
%	−64	−48		−22	ns

[1]Loading regimes: I, incisor loading; right P^3 and right M^2, unilateral loading of right P^3 and right M^2; left P^3 and left M^2, unilateral loading of left P^3 and M^2.
*% = statistically significant ($P < 0.05$) changes in ϵ_2 magnitude caused by cutting the septa expressed as a percentage of ϵ_2 magnitude before the septa were cut. ns = no significant difference between the values recorded before and after cutting the septa.

TABLE 5. Mean ϵ_1/ϵ_2 magnitude (and standard deviation) (in microstrain units) recorded from the interorbital region and lateral and medial surfaces of the left postorbital bar before (B) and after (A) cutting postorbital septa (n = 10 loadings before and after)[1]

	I	Right P^3	Right M^2	Left P^3	Left M^2
Interorbital region					
B	0.9 (.02)	1.2 (.07)	2.3 (.36)	1.0 (.04)	1.7 (.13)
A	0.9 (.01)	1.3 (.05)	1.7 (.09)	1.0 (.03)	1.2 (.03)
Postorbital bar (lateral)					
B	1.6 (.09)	1.7 (.19)	1.6 (.18)	2.2 (.07)	2.1 (.05)
A	1.9 (.06)	0.6 (.04)	0.5 (.04)	2.6 (.11)	2.1 (.06)
Postorbital bar (medial)					
B	0.8 (.12)	0.8 (.07)		0.6 (.03)	0.6 (.02)
A	0.6 (.06)	1.5 (.47)	1.7 (.19)	0.6 (.03)	0.6 (.05)

[1] Loading regimes: I, incisor loading; right P^3 and right M^2, unilateral loading of right P^3 and right M^2; left P^3 and left M^2, unilateral loading of left P^3 and M^2.

TABLE 6. Mean (and standard deviation) angle of ϵ_1 (in degrees) recorded from the interorbital region and lateral and medial surfaces of the left postorbital bar before (B) and after (A) cutting postorbital septa (n = 10 loadings before and after)[1]

	I	Right P^3	Right M^2	Left P^3	Left M^2
Interorbital region					
B	−86 (0.4)	−86 (0.6)	−84 (0.6)	−86 (0.7)	−86 (1.2)
A	−85 (0.2)	−87 (0.5)	−87 (0.9)	−84 (0.8)	−84 (0.5)
Postorbital bar (lateral)					
B	17 (0.7)	20 (1.5)	21 (1.7)	−6 (0.6)	−22 (0.4)
A	6 (0.6)	84 (1.0)	84 (0.8)	−6 (0.5)	−11 (0.4)
Postorbital bar (medial)					
B	−12 (1.4)	−19 (1.3)		11 (1.4)	19 (0.9)
A	13 (1.9)	−90 (3.6)	−85 (2.0)	9 (1.1)	5 (1.3)

[1] Loading regimes: I, incisor loading; right P^3 and right M^2, unilateral loading of right P^3 and right M^2; left P^3 and left M^2, unilateral loading of left P^3 and M^2.

surface and compressive strains highest on the medial surface (Table 5). These data suggest that the septum does not function to reduce strain levels in the lateral orbital wall under conditions of unilateral loading of the premolars, although it does appear to reduce strain magnitudes slightly in the interorbital region.

Loading M^2. During loading of the M^2, cutting the septum causes increased γ-max magnitudes in the interorbital region and the working side postorbital bar, particularly on the lateral surface (Table 2). There is no change in the amount of strain along the lateral surface of the balancing side orbital wall and increased γ-max magnitudes in the interorbital region (Table 2). These data suggest that during loading of M^2 the presence of an intact postorbital septum reduces strain magnitudes in the interorbital region and along the working-side lateral orbital wall.

DISCUSSION OF IN VITRO RESULTS

Strain orientations

The laterally directed orientation of ϵ_1 in the interorbital region during unilateral loading of the postcanine tooth row, whether the septum is present or not, does not support the facial-torsion hypothesis, which predicts principal tension to be oriented at 45° during unilateral loading of the tooth row. These data cannot be invoked either to corroborate or falsify the transverse-bending and tension hypotheses because the loading regimes posited by these hypotheses were not replicated during the in vitro experiment. Clearly, however, dorsally directed forces acting anywhere along the maxillary tooth row appear to be associated with rostrocaudal compression of the interorbital region, whether the postorbital septum is present or not.

Both before and after cutting the postor-

bital septa, unilateral loading of the tooth row (P^3 and M^2) is associated with orthogonally oriented strains on medial and lateral surfaces of the working side postorbital bar (i.e., ϵ_1 is dorsoventrally oriented on the lateral surface and rostrocaudally oriented on the medial surface). This suggests that the working side lateral orbital wall (i.e., that which is ipsilateral to the load) is being dorsoventrally compressed and buckled. Before the septa are cut, the pattern of strain on the balancing side is similar to that on the working side (i.e., principal tension on the lateral surface is oriented predominantly dorsoventrally, while that on the medial surface is oriented predominantly rostrocaudally). In contrast, cutting the septa radically alters the pattern of strain along the balancing side postorbital bar. After cutting, principal tensile strains on the balancing side are oriented orthogonal to those on the working side (i.e., principal tension on the lateral surface is oriented predominantly rostrocaudally, while that on the medial surface is oriented predominantly dorsoventrally). This suggests that in the absence of the septum the balancing side lateral orbital wall is being dorsoventrally tensed.

Taken together, these results suggest that, whether the septum is intact or not, incisor loading bends the face upward in the sagittal plane, compressing the dorsal interorbital region rostrocaudally and the lateral orbital walls dorsoventrally. The lateral orbital walls appear to be buckled as a result. Unilateral loading of the tooth row appears to bend the face dorsally in the sagittal plane, compressing the interorbital region rostrocaudally and the working side lateral orbital wall dorsoventrally. The pattern of strain along the intact balancing side lateral orbital wall is suggestive of dorsoventral compression and buckling, although in a slightly different plane to that in which the working side lateral orbital wall is bent. After the postorbital septa are cut, unilateral loading still results in dorsoventral compression and buckling of the working side lateral orbital wall, but the balancing side wall is dorsoventrally tensed and unbent. These data suggest that the septum does not prevent the entire face from twisting on the braincase but may prevent the palate from "seesawing" side to side about the interorbital region due to the bite force (Fig. 10).

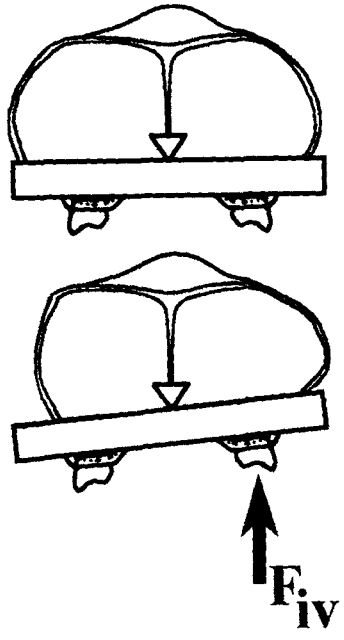

Fig. 10. Diagram illustrating loading regime hypothesized to be associated with unilateral loading of the toothrow in vitro after cutting the postorbital septa. A dorsally directed force applied to the tooth row in vitro (F_{iv}) is hypothesized to buckle the lateral orbital wall ipsilateral to the load (the working side), while the balancing side is unbent.

Strain magnitudes

Under incisor loading, an intact postorbital septum is actually associated with *increased* bone strain levels in either the interorbital region or lateral orbital wall, suggesting that the postorbital septum does not reinforce the circumorbital region against this kind of loading regime. Under unilateral loading of the premolars, an intact postorbital septum does not reduce bone strain levels in the lateral orbital walls, although it does reduce strain magnitudes slightly in the interorbital region. Finally, under loading of the M^2, an intact postorbital septum reduces strain magnitudes in the interorbital region and working side lateral orbital wall but does not change strain mag-

nitudes in the balancing side lateral orbital wall.

IN VIVO RESULTS

Interorbital region

Strain gage position and orientation. Strain gages were placed in the interorbital region in three experiments: 7, 8, and 13 (Table 1). A problem was encountered while recording the orientations of the principal strains recorded from the interorbital region in experiment 8. We believe that the lead wire plugs from the A- and C-elements were inadvertently switched, and therefore the data from these elements were recorded on the wrong channels of the tape recorder. If so, the direction of ϵ_1 is affected by this switch, but the strain magnitudes of ϵ_1, ϵ_2, and γ-max are not. Consequently, we have excluded the strain orientation data recorded during that experiment but have retained the strain magnitude data (Table 8a).

An effort was made to position the strain gages on the midline of the skull, but there was nonetheless some unavoidable variability in gage position. The interorbital strain gage in experiment 7 was positioned slightly to the right of the midline (Fig. 11). Similarly, the interorbital gage in experiment 8 was also positioned slightly to the right of the midline. This gage was also positioned slightly rostral to the gage in experiment 7. The position of the interorbital gage in experiment 13 was rostral to those of experiments 7 and 8 (Fig. 11), but its exact position relative to the midline is unclear, as the head was greatly canted relative to the radiographic film when the radiograph was made.

Tables 7a and 9 present descriptive statistics for the orientation of peak ϵ_1 recorded from the interorbital region during mastication and incision of hard prune, hard apricot, and gummy bear in experiments 7 and 13. The orientations of mean peak ϵ_1 recorded during incision and mastication on left and right sides in experiments 7 and 13 are indicated in Figure 11.

Strain magnitudes. Descriptive statistics for the magnitudes of the principal strains and γ-max recorded from the interorbital region are given in Tables 7a, 8a, and 9. In the interorbital region, mean values for ϵ_1 range from 19–168 $\mu\epsilon$; mean values for ϵ_2 range from -49 $\mu\epsilon$ to -177 $\mu\epsilon$. The largest values recorded were 356 $\mu\epsilon$ in tension and -368 $\mu\epsilon$ in compression. The ratio of ϵ_1/ϵ_2 ranges from 0.2–1.2, with the majority of values being less than 1 and the grand mean from all experiments combined being 0.5. In experiments 7 and 8, the magnitudes of the principal strains recorded during incision are higher than those recorded during mastication (Tables 7a, 8a). The results from experiment 13 indicate the opposite tendency (Table 9). The strain magnitudes recorded during experiments 7 and 8 tend to be higher when the animal was chewing on the left than chewing on the right.

Strain orientation. Figure 11 illustrates for experiments 7 and 13 the mean orientation of ϵ_1 recorded from the interorbital region during incision and mastication of all hard foods (hard prune, hard apricot, gummy bear). In experiment 7 (Fig. 11) ϵ_1 is oriented laterally and somewhat rostrally on the left during both chewing on the right and chewing on the left; during incision, ϵ_1 is oriented laterally and slightly rostrally on the left. Furthermore, ϵ_1 is more rostrally oriented on the left during chewing on the left than during chewing on the right (Fig. 11). In experiment 13, ϵ_1 is oriented almost perpendicular to the mid-sagittal plane during incision (Fig. 11). During chewing on the right ϵ_1 is oriented latero-rostrally and to the left, whereas during chewing on the left ϵ_1 is oriented latero-rostrally and to the right.

Comparisons of these mean values reveal that in experiment 7 mean orientation of ϵ_1 recorded during chewing on the left is significantly different from that recorded during incision and chewing on the right, but the mean orientation recorded during incision is not significantly different from the mean recorded during chewing on the right. In experiment 13, the orientations of ϵ_1 recorded during chewing on the left, during chewing on the right, and during incision are all significantly different from one another.

Postorbital bar (Lateral surface)

Strain gage position and orientation. Strain gages were bonded to the lateral surface of the postorbital bar in experiments

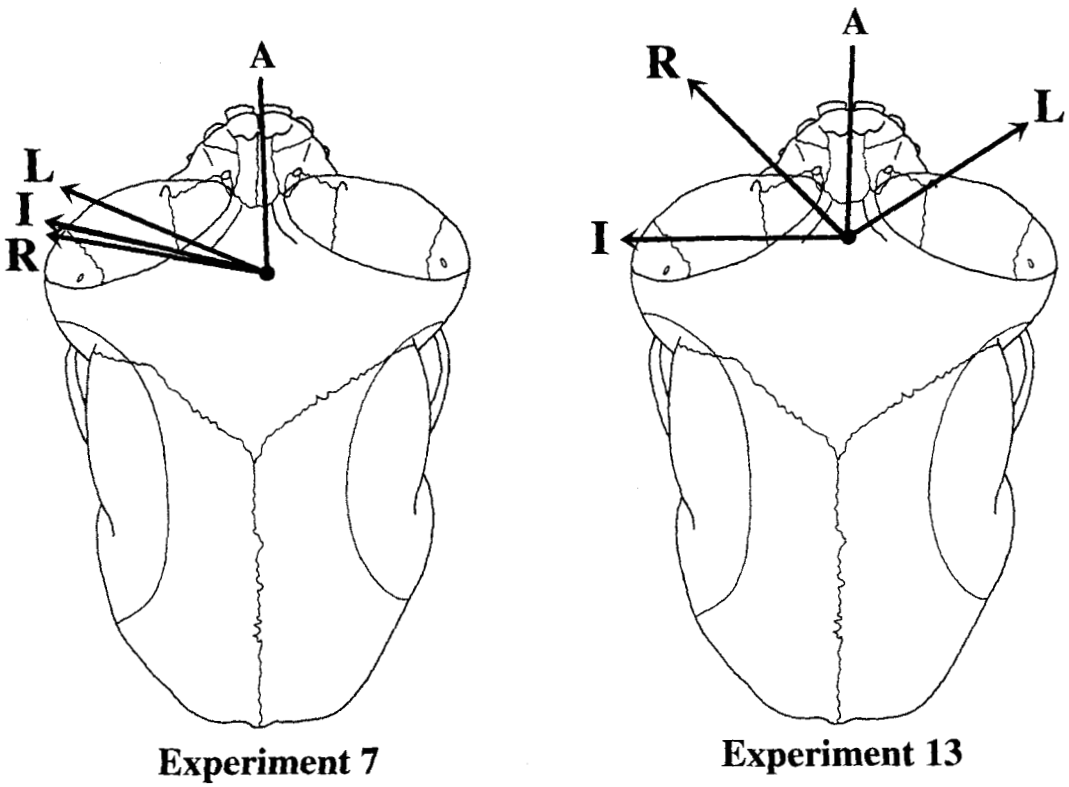

Fig. 11. Orientations of ϵ_1 recorded from the interorbital region during experiments 7 and 13. A, orientation of A-element; I, orientation of ϵ_1 during incision; L, orientation of ϵ_1 during chewing on the left; R, orientation of ϵ_1 during chewing on the right.

7–10 (Table 1). There is variation in gage position and orientation among the experiments. In experiment 7 the gage was bonded to the postorbital bar approximately midway between the lateral orbital margin and the temporal line and at the height of mid-orbit (Fig. 12). In experiment 8 the gage was positioned much lower on the lateral surface of the bar but again approximately midway between the lateral orbital margin and the temporal line (Fig. 12). The gages in experiments 9 and 10 were positioned more rostrally, close to the lateral orbital margin. The gage in experiment 10 was placed at about mid-orbit, the gage in experiment 9 further ventrally (Fig. 13).

Strain magnitude. Tables 7a, 8a, 10, and 11 give descriptive statistics for the magnitudes of the principal strains and γ-max recorded from the lateral surface of the postorbital bar. Mean values for ϵ_1 range from 45–688 $\mu\epsilon$, and mean values for ϵ_2 range from -66 $\mu\epsilon$ to -637 $\mu\epsilon$. The largest values recorded were 873 $\mu\epsilon$ in tensile strain and -817 $\mu\epsilon$ in compressive strain (Table 7a). The ratio of ϵ_1/ϵ_2 recorded from the working side postorbital bar ranges from 0.4–1.4; the balancing side ratios range from 0.5–1.1.

Strain orientation. Figures 12 and 13 illustrate the mean orientation of ϵ_1 recorded from the postorbital bar during mastication and incision of all hard foods (grand mean of means recorded during processing of hard prune, hard apricot, gummy bear) when the strain gage was on the working side (W) and the balancing side (B) and during incision (I). For experiments 7 and 8 (Fig. 12) and experiment 10 (Fig. 13), ϵ_1 is oriented mostly upward and slightly forward; in experiment 9, ϵ_1 is oriented more forward than in these

TABLE 7a. Descriptive statistics for peak ϵ_1 orientation and peak ϵ_1, ϵ_2, ϵ_1/ϵ_2, and γ-max magnitudes recorded from the interorbital region and postorbital bar of owl monkey 1 during experiment 7

		ϵ_1			ϵ_2			Ratio ϵ_1/ϵ_2		γ-max			Orientation of ϵ_1			
Subject, food, and side	n	Mean	SD	Max	Mean	SD	Max	Mean	Max	Mean	SD	Max	Mean	SD	Max	Min
Owl monkey 1, interobital region																
Mastication																
Hard prune																
Chew right	72	32	12	58	−49	22	−102	0.8	.52	82	31	154	78	9.8	98	50
Chew left	108	33	13	59	−74	38	−157	0.5	.19	108	50	215	66	5.6	83	52
Hard apricot																
Chew right	22	35	8	48	−61	27	−118	0.7	.31	96	31	161	77	8.1	96	58
Chew left	23	42	12	69	−101	37	−181	0.4	.13	143	48	250	69	5.1	77	62
Incision																
Hard prune	29	78	24	105	−177	59	−245	0.4	.08	255	81	346	76	1.8	79	72
Hard apricot	14	58	27	89	−148	68	−234	0.4	.09	206	93	323	75	1.7	78	72
Owl monkey 1, right postorbital bar																
Mastication																
Hard prune																
Chew right (W)	72	411	98	629	−391	99	−623	1.0	.05	802	196	1,252	−14	2.1	−8	−23
Chew left (B)	108	442	136	683	−409	130	−646	1.1	.04	851	266	1,329	−21	2.5	−12	−27
Hard apricot																
Chew right (W)	22	413	95	569	−394	86	−537	1.0	.03	807	180	1,106	−16	2.8	−10	−20
Chew left (B)	23	478	108	680	−453	100	−636	1.0	.02	931	209	1,316	−21	2.0	−16	−23
Incision																
Hard prune	29	688	175	873	−637	168	−817	1.1	.04	1,324	434	1,690	−20	1.1	−16	−22
Hard apricot	14	585	205	809	−540	199	−753	1.1	.06	1,126	404	1,562	−19	1.9	−15	−21

TABLE 7b. Ratio of postorbital bar γ-max to interorbital region γ-max recorded from owl monkey 1 during experiment 7

	n	Mean	SD
Mastication			
Hard prune			
Chew right (W)	72	10.5	2.5
Chew left (B)	108	8.8	2.6
Hard apricot			
Chew right (W)	22	8.7	1.3
Chew left (B)	23	7.0	1.8
Incision			
Hard prune	29	5.4	1.2
Hard apricot	14	6.0	1.6

[1]W, working side; B, balancing side; refer to postorbital bar only.

other experiments (Fig. 13). In experiments 7–9 the orientation of ϵ_1 on the balancing side is forward of both those recorded along the working side and during incision (Figs. 12, 13). In experiment 10 the orientation of ϵ_1 on the working side is rostral to the mean orientations recorded from the balancing side and during incision (Fig. 13).

Comparisons among the means within each experiment reveal the following: in experiments 7–9 the mean orientations of ϵ_1 recorded on the balancing and working sides, as well as during incision, are all significantly different from one another; in experiment 10, the mean orientations of ϵ_1 recorded on the balancing side and during incision are not significantly different from one another, although both are significantly different from the mean working side value. Notably, although the mean value of ϵ_1 during incision is significantly different from the balancing side values in experiments 7–9, the mean incision value is always more similar to the balancing side mean value than it is to the working side mean (see Tables 9, 10).

Postorbital septum (Medial surface)

Strain gage position and orientation. In experiments 4 and 6, a single rosette gage was bonded to the orbital surface of the left postorbital septum (Table 1). An effort was made to orient the A-element perpendicular to the orbital margin. Unfortunately, it is not possible from the radiographs to determine whether there are significant differences in gage position between the two experiments, nor is it possible to determine the exact orientation of the gages from the radiographs. The strain orientations in Figure 14 are drawn assuming that the A-elements were indeed oriented perpendicular to the lateral orbital margin.

Strain magnitudes. Table 12 gives descriptive statistics for the various strain val-

TABLE 8a. Descriptive statistics for peak ϵ_1 orientation recorded from the postorbital bar and for peak ϵ_1, ϵ_2, ϵ_1/ϵ_2, and γ-max magnitudes recorded from the postorbital bar and interorbital region of owl monkey 2 during experiment 8 postorbital bar, while those for the interorbital region are omitted due to recording problems (see text for details)[1]

		ϵ_1			ϵ_2			Ratio ϵ_1/ϵ_2		γ-max			Orientation of ϵ_1			
Subject, food, and side	n	Mean	SD	Max	Mean	SD	Max	Mean	Max	Mean	SD	Max	Mean	SD	Max	Min
Owl monkey 2, interobital region																
Mastication																
Hard prune																
Chew right	81	20	6	33	−72	24	−115	0.3	.15	92	27	139				
Chew left	89	35	15	114	−105	40	−194	0.3	.10	140	52	248				
Gummy bear																
Chew right	78	19	7	35	−88	18	−137	0.2	.06	107	23	168				
Chew left	52	24	13	47	−87	51	−170	0.3	.11	111	63	217				
Incision																
Hard prune	81	48	19	89	−168	85	−340	0.3	.09	216	103	425				
Gummy bear	8	40	10	54	−120	46	−223	0.3	.06	160	54	277				
Owl monkey 2, postorbital bar																
Mastication																
Hard prune																
Chew right (W)	81	287	84	447	−221	72	−378	1.3	.20	508	154	825	−24	3.9	−15	−7
Chew left (B)	89	275	102	468	−307	126	−549	0.9	.17	582	227	1017	−38	2.9	−25	−46
Gummy bear																
Chew right (W)	78	314	40	408	−231	49	−356	1.4	.16	545	87	729	−22	3.1	−17	−31
Chew left (B)	52	225	123	409	−246	154	−484	1.0	.28	471	277	893	−34	5.8	−15	−39
Incision																
Hard prune	81	346	152	658	−383	178	−745	0.8	.08	729	330	1403	−36	2.1	−27	−41
Gummy bear	8	251	79	426	−285	79	−526	0.9	.04	536	183	952	−36	1.0	−36	−39

[1] Interorbital region data on ϵ_1 orientation are omitted due to recording problems. (See text for details.)

TABLE 8b. Ratios of γ-max recorded from the postorbital bar over γ-max recorded from the interorbital region from owl monkey 2 during experiment 8[1,2]

	n	Mean	SD
Mastication			
Hard prune			
Chew right (W)	81	5.6	1.0
Chew left (B)	89	4.2	0.9
Gummy bear			
Chew right (W)	78	5.2	0.6
Chew left (B)	52	4.3	0.9
Incision			
Hard prune	81	3.5	0.9
Gummy bear	8	3.4	0.2

[1] Interorbital region data on ϵ_1 orientation are omitted due to recording problems. (See text for details.)
[2] W, working side; B, balancing side; refer to postorbital bar only.

ues recorded from the medial surface of the postorbital septum. Mean values for ϵ_1 range from 42–302 $\mu\epsilon$, and mean values for ϵ_2 range from −58 $\mu\epsilon$ to −231 $\mu\epsilon$. The largest values recorded were 414 $\mu\epsilon$ in tensile strain and −345 $\mu\epsilon$ in compressive strain. The mean ratio of ϵ_1/ϵ_2 recorded from the postorbital septum on the working side ranges from 0.7–0.9, whereas the mean balancing side ratios range from 0.9–1.7. The incision ratios, which are intermediate in value, range from 0.9–1.3.

Strain orientation. Figure 14 illustrates the mean orientation of ϵ_1 recorded from the medial surface of the postorbital septum

TABLE 9. Descriptive statistics for peak ϵ_1, ϵ_2, ϵ_1/ϵ_2, and γ-max magnitudes as well as for ϵ_1 orientation recorded from owl monkey 1 during experiment 13

		ϵ_1			ϵ_2			Ratio ϵ_1/ϵ_2		γ-max			Orientation of ϵ_1			
Subject, food, and side	n	Mean	SD	Max	Mean	SD	Max	Mean	Max	Mean	SD	Max	Mean	SD	Max	Min
Owl monkey 1, interobital region																
Mastication																
Gummy Bear																
Chew left	158	168	94	356	−145	77	−307	1.2	.94	313	170	654	−57	6	−26	−88
Chew right	117	109	58	261	−128	71	−368	0.9	.12	237	128	629	47	11	78	24
Incision																
Gummy bear	55	101	46	282	−115	39	−233	0.9	.17	216	83	515	92	14	124	58

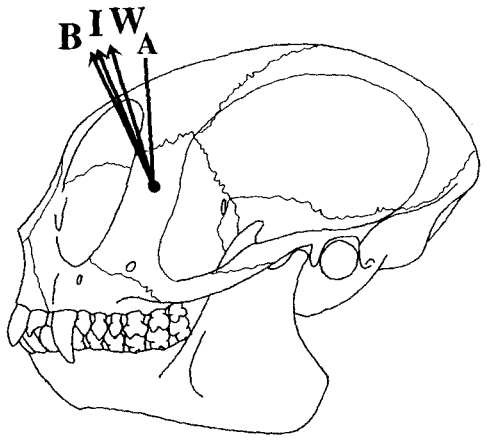

Experiment 7

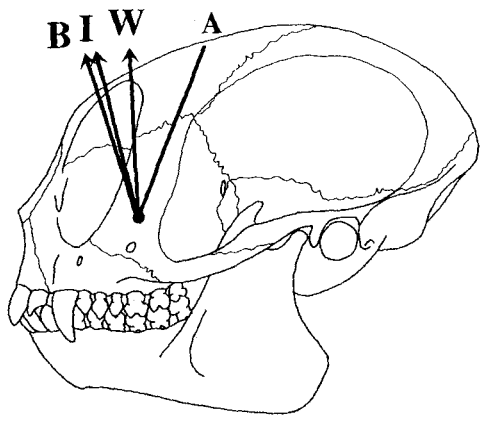

Experiment 8

Fig. 12. Orientations of ● recorded from the lateral surface of the postorbital bar during experiments 7 and 8. A, orientation of A-element; I, orientation of ϵ_1 during incision; L, orientation of ϵ_1 during chewing on the left; R, orientation of ϵ_1 during chewing on the right.

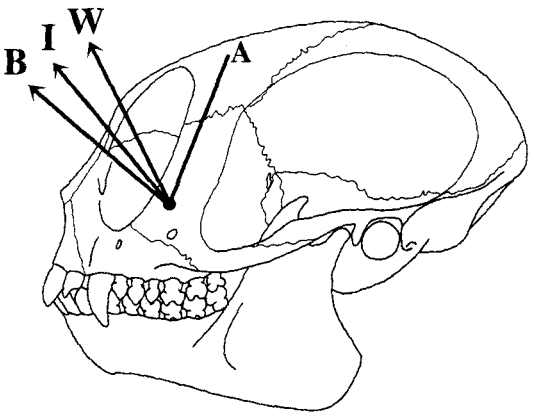

Experiment 9

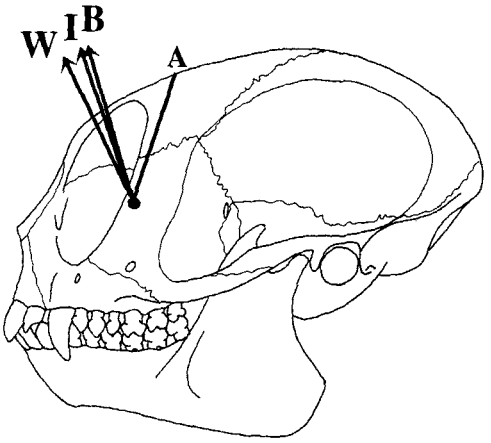

Experiment 10

Fig. 13. Orientations of ϵ_1 recorded from the lateral surface of the postorbital bar during experiments 9 and 10. A, orientation of A-element; I, orientation of ϵ_1 during incision; L, orientation of ϵ_1 during chewing on the left; R, orientation of ϵ_1 during chewing on the right.

during mastication and incision of hard foods in experiments 4 (owl monkey 1) and 6 (owl monkey 2). All ϵ_1 orientations on the medial surface of the postorbital septum are more rostrocaudal than dorsoventral. The mean orientation of ϵ_1 on the balancing side is more superiorly oriented posteriorly than the mean orientation of ϵ_1 during incision, and both are more superiorly oriented posteriorly than the mean orientation of ϵ_1 on the working side. The mean orientation of ϵ_1 during incision is always intermediate to the working and balancing side orientations. These mean orientations of ϵ_1 in the postorbital septum are all significantly different from one another. In experiments 4 and 6, the mean orientation of ϵ_1 during incision is more similar to the mean balancing side orientation than to the working side orientation.

Comparison of simultaneous strain magnitudes

In experiments 7 and 8, strain data were gathered simultaneously from the right postorbital bar and from the interorbital region. In experiments 9 and 10, strain data were gathered simultaneously from the left

TABLE 10. Descriptive statistics for peak ϵ_1, ϵ_2, ϵ_1/ϵ_2, and γ-max magnitudes recorded from owl monkey 2 during experiment 9, with descriptive statistics for ϵ_1 orientation recorded from the postorbital bar and the ratios of γ-max recorded from the postorbital bar over γ-max recorded from the mandibular corpus[1]

		ϵ_1			ϵ_2			Ratio ϵ_1/ϵ_2		γ-max			Orientation of ϵ_1			
Subject, food, and side	n	Mean	SD	Max	Mean	SD	Max	Mean	Max	Mean	SD	Max	Mean	SD	Max	Min
Owl monkey 2, postorbital bar																
Mastication																
Hard prune																
Chew left (W)	84	271	90	458	−217	75	−377	1.3	.11	488	165	835	46	2.2	51	36
Chew right (B)	105	78	43	226	−125	38	−252	0.6	.24	203	75	478	71	9.9	93	40
Hard apricot																
Chew left (W)	43	294	83	512	−291	112	−605	1.0	.19	586	187	1,117	46	3.9	56	40
Chew right (B)	43	65	17	104	−102	29	−145	0.7	.22	168	39	220	72	8.3	87	40
Gummy bear																
Chew left (W)	57	338	87	497	−277	70	−404	1.2	.03	615	156	901	47	1.0	50	43
Chew right (B)	76	58	36	316	−114	31	−260	0.5	.15	172	64	576	71	6.1	85	48
Incision																
Hard prune	46	127	55	238	−156	62	−277	0.8	.12	283	116	503	60	5.1	76	45
Hard apricot	18	193	71	412	−265	83	−433	0.7	.22	458	141	762	53	5.5	62	43
Gummy bear	5	148	34	207	−218	34	−275	0.7	.04	366	68	482	60	1.5	62	58

		Ratio of corpus γ-max to postorbital bar γ-max	
Owl monkey 2, mandibular corpus			
Mastication			
Hard prune		Mean	SD
Chew left (W)	84	1.6	0.3
Chew right (B)	105	3.3	1.0
Hard apricot			
Chew left (W)	43	1.3	0.3
Chew right (B)	43	3.0	0.8
Gummy bear			
Chew left (W)	57	1.4	0.2
Chew right (B)	76	4.0	0.8
Incision			
Hard prune	46	2.4	0.5
Hard apricot	18	2.0	0.5
Gummy bear	5	2.8	0.1

[1] W, working side; B, balancing side.

postorbital bar and from the left mandibular corpus in the region of M_1 (Table 1). Descriptive statistics for γ-max recorded during experiments 7 and 8 are given in Tables 7a and 8a; the ratios of postorbital bar γ-max to interorbital region γ-max are given in Tables 7b and 8b. Descriptive statistics for γ-max and the ratios of mandibular corpus to postorbital bar γ-max recorded during experiments 9 and 10 are given in Tables 10 and 11.

These data demonstrate that there is much more strain in the postorbital bar than in the interorbital region and that there is usually (although not always) more strain in the mandibular corpus than in the postorbital bar. During these experiments, mean γ-max strains recorded in the interorbital region during mastication of hard food objects (dried apricot, dried prune, gummy bear) range from 82–255 $\mu\epsilon$, with a grand mean of 143 $\mu\epsilon$; mean γ-max strains in the postorbital bar range from 111–1,324 $\mu\epsilon$, with a grand mean of 510 $\mu\epsilon$, and mean γ-max strains in the mandibular corpus range from 508–1,814 $\mu\epsilon$, with a grand mean of 987 $\mu\epsilon$. The ratio of postorbital bar γ-max/interorbital γ-max is larger on the working side than on the balancing side and during incision. During mastication, the ratio of mandibular corpus γ-max/postorbital bar γ-max is larger on the balancing side than on the working side; during incision the ratio is larger than on the working side but smaller than on the balancing side.

Comparison of strain magnitudes from other experiments

Although strain data were not gathered from the postorbital septum at the same time as strain data were gathered from other parts of the face, some general observations

TABLE 11. Descriptive statistics for peak ϵ_1, ϵ_2, ϵ_1/ϵ_2, and γ-max magnitudes recorded from owl monkey 1 during experiment 10, with descriptive statistics for ϵ_1 orientation recorded from the postorbital bar and the ratios of γ-max recorded from the postorbital bar over γ-max recorded from the mandibular corpus[1]

		ϵ_1			ϵ_2			Ratio ϵ_1/ϵ_2		γ-max			Orientation of ϵ_1			
Subject, food, and side	n	Mean	SD	Max	Mean	SD	Max	Mean	Max	Mean	SD	Max	Mean	SD	Max	Min
Owl monkey 1, postorbital bar																
Mastication																
Hard prune																
Chew left (W)	20	60	14	83	−157	35	−217	0.4	.08	217	48	296	44	2.7	48	36
Chew right (B)	14	54	14	77	−107	26	−155	0.5	.04	162	40	232	35	1.5	38	32
Gummy bear																
Chew left (W)	83	61	18	95	−160	44	−242	0.4	.06	221	61	337	43	1.3	46	38
Chew right (B)	57	45	16	87	−66	24	−118	0.7	.20	111	36	199	35	6.0	52	21
Incision																
Hard prune	2	118	12	126	−146	31	−168	0.8	.26	246	46	278	37	8.0	42	31
Gummy bear	27	102	16	130	−165	27	−220	0.6	.07	267	41	345	36	4.0	43	24

													Ratio of corpus γ-max to postorbital bar γ-max	
Owl monkey 1, mandibular corpus														
Mastication														
Hard prune													Mean	SD
Chew left (W)	20	489	125	711	−823	168	−1,048			1,312	291	1,759	6.1	0.7
Chew right (B)	14	360	102	509	−736	195	−1,015			1,096	297	1,506	6.7	0.7
Gummy bear														
Chew left (W)	83	450	96	610	−748	153	−1,021			1,198	248	1,631	5.6	0.7
Chew right (B)	57	280	99	475	−519	171	−848			800	268	1,323	7.2	1.0
Incision														
Hard prune	2	630	66	676	−1,184	146	−1,287			1,814	211	1,963	7.4	0.5
Gummy bear	27	613	85	810	−1,191	152	−1,481			1,805	231	2,268	6.8	0.7

[1] W, working side; B, balancing side.

TABLE 12. Descriptive statistics for ϵ_1 orientation and peak ϵ_1, ϵ_2, ϵ_1/ϵ_2, and γ-max magnitudes recorded from the medial surface of the postorbital septum during experiments 4 and 6 on owl monkeys 1 and 2

		ϵ_1			ϵ_2			Ratio ϵ_1/ϵ_2		γ-max			Orientation of ϵ_1			
Subject, food, and side	n	Mean	SD	Max	Mean	SD	Max	Mean	Max	Mean	SD	Max	Mean	SD	Max	Min
Owl monkey 1, postorbital septum (medial surface), experiment 4																
Mastication																
Hard prune																
Chew left (W)	40	42	19	70	−58	21	−88	0.7	.20	101	39	154	−26	14.8	3	−48
Chew right (B)	115	97	66	309	−108	68	−320	0.9	.15	206	133	629	−57	5.9	−40	−64
Hard apricot																
Chew left (W)	40	47	15	84	−56	22	−104	0.9	.18	103	36	188	−17	17.0	23	−42
Chew right (B)	30	118	74	252	−129	79	−269	0.9	.11	248	152	521	−60	4.8	−44	−65
Gummy bear																
Chew left (W)	18	46	15	77	−61	18	−92	0.8	.20	107	30	156	−24	9.8	−6	−41
Chew right (B)	20	119	53	234	−122	55	−234	1.0	.05	241	108	468	−60	2.6	−51	−63
Incision																
Hard prune	52	185	77	297	−202	77	−307	0.9	.08	390	154	601	−56	1.4	−52	−58
Hard apricot	23	188	65	268	−195	66	−274	0.9	.04	383	131	539	−56	2.2	−51	−59
Gummy bear	6	167	42	217	−187	48	−231	0.9	.06	354	89	448	−56	0.5	−55	−56
Owl monkey 2, postorbital septum (medial surface), experiment 6																
Mastication																
Hard prune																
Chew left (W)	138	179	46	288	−199	50	−308	0.9	.14	378	92	596	−52	3.3	−38	−61
Chew right (B)	105	197	83	355	−120	50	−214	1.6	.20	316	132	561	−66	3.2	−45	−71
Hard apricot																
Chew left (W)	84	164	53	290	−197	43	−295	0.8	.21	361	89	547	−48	8.3	−14	−64
Chew right (B)	79	242	96	375	−143	59	−224	1.7	.17	386	154	590	−68	2.0	−62	−73
Incision																
Hard prune	13	302	55	406	−231	42	−297	1.3	.24	533	81	669	−59	4.0	−51	−62
Hard apricot	49	261	112	414	−197	89	−345	1.3	.22	458	197	740	−61	3.4	−53	−69

[1] W, working side; B, balancing side.

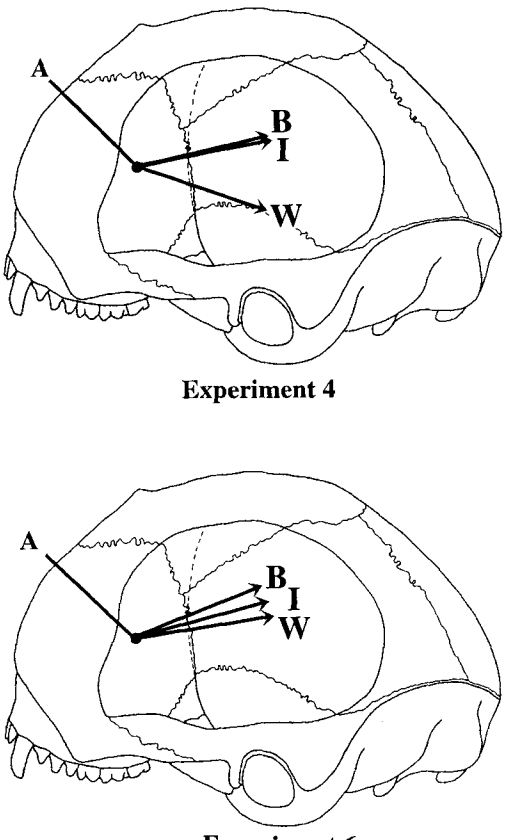

Fig. 14. Orientations of ϵ_1 recorded from the medial surface of the postorbital septum during experiments 4 and 6. A, orientation of A-element; I, orientation of ϵ_1 during incision; L, orientation of ϵ_1 during chewing on the left; R, orientation of ϵ_1 during chewing on the right.

are possible. The mean γ-max recorded from the postorbital septum during mastication of hard food objects (dried apricot, dried prune, gummy bear) ranged from 101–533 $\mu\epsilon$, with a grand mean of 143 $\mu\epsilon$. These results are similar to those obtained in the interorbital region (vide supra). The strain magnitudes in the postorbital septum can therefore be tentatively concluded to be generally lower than those in the postorbital bar and mandibular corpus.

DISCUSSION OF IN VIVO BONE STRAIN RESULTS

As discussed above, data on strain orientation allow us to determine whether the face is loaded as predicted by the three hypotheses evaluated here: the facial-torsion hypothesis, the transverse-bending hypothesis, and the tension hypothesis. In this section, in vivo bone strain data are compared with the results of the in vitro experiment and with the theoretical predictions derived from modeling the skull as a simple structural member.

The facial torsion hypothesis

The directional data recorded from the interorbital region during experiment 7 (Fig. 11) do not agree with the theoretical predictions of the facial-torsion model when the skull is modeled as a simple cylinder (Fig. 1) (cf. Greaves, 1985), nor do they resemble the strain orientations recorded during actual twisting of the skull in vitro (Fig. 7). The difference between the mean orientations of ϵ_1 during chewing on the left and chewing on the right is much less than the 90° predicted by the theoretical model (Table 7a), and the direction of ϵ_1 is lateral to the left and slightly rostral during chewing both on the left and right as well as during incision. However, the orientations of ϵ_1 recorded during experiment 13 provide some support for the facial-torsion hypothesis (Fig. 11). The direction of ϵ_1 is lateral and rostral to the left when the animal chews on the right and lateral and rostral to the right when chewing on the left, as predicted by the facial torsion hypothesis. Moreover, the difference between the mean orientations of ϵ_1 during chewing on the left and chewing on the right is 104° (Table 9), fairly close to the 90° predicted by the theoretical model.

One explanation for the difference between these two experiments is differences in strain gage position: the interorbital strain gage in experiment 13 was positioned rostral to that in experiment 7 (Fig. 11). If this explanation is correct, the significant variability in strain orientations across the interorbital region falsifies the facial-torsion hypothesis, because if twisting of the face on the braincase is an important loading regime, strain orientations predicted by the hypothesis should be observed at all points in the interorbital region.

The directional data gathered from the lateral orbital wall in experiments 4 and 6–10 also do not match the predictions of the fa-

cial-torsion hypothesis (Fig. 1A). Moreover, contrary to the predictions of the facial-torsion hypothesis, the difference between the mean orientations on the working and balancing sides in all four experiments is considerably less than 90° (Tables 10, 11).

In sum, these data indicate that either the dominant loading regime in the face during unilateral biting and mastication is not torsion of the face on the braincase or, because of its complex shape, the skull should not be modeled as a simple cylinder. If the face of owl monkeys does indeed twist on the braincase during unilateral biting and mastication, the magnitude of this twisting is smaller than that of other loading regimes, suggesting that facial torsion is not a very important loading regime.

The transverse-bending hypothesis

If the interorbital area to be analyzed is assumed to lie rostral to the bending axis of neutrality, the interorbital bone strain data during incision provide some corroboration for the transverse-bending hypothesis. The orientation of ϵ_1 is laterad during incision, being perpendicular to the mid-sagittal plane of the skull in experiment 13 (Fig. 11) and near perpendicular in experiment 7 (Fig. 11). However, the bone strain data recorded from the interorbital region during mastication do not corroborate the transverse-bending hypothesis, because ϵ_1 is oriented too far rostrad to be indicative of pure transverse bending.

The orientations of ϵ_1 recorded from the lateral orbital wall also do not corroborate the transverse-bending hypothesis. ϵ_1 on the lateral surface of the postorbital bar is oriented predominantly vertically during mastication and incision, orthogonal to the direction predicted by the transverse-bending hypothesis (Figs. 12, 13). The directional data obtained from the postorbital bar in experiment 9 (Fig. 12) come closest to the orientations predicted by this hypothesis but nevertheless deviate considerably from the predicted values. Finally, ϵ_1 on the medial surface of the postorbital septum has a predominantly rostrocaudal orientation (Fig. 14), not the vertical orientation predicted by the transverse-bending hypothesis (cf. Fig. 2).

In sum, data on the orientations of ϵ_1 do not corroborate the hypothesis that the circumorbital region is bent in a transverse plane during mastication and incision.

The tension hypothesis

The orientations of ϵ_1 recorded from the interorbital region do not support the hypothesis that the lateral orbital wall is pulled ventrally during mastication. ϵ_1 orientations recorded during mastication in experiments 7 and 13 are oriented rostrally to varying degrees (Fig. 11), not directly laterally as predicted by the tension hypothesis (Fig. 4). Only during incision in experiment 13 is ϵ_1 oriented directly laterally as predicted.

The orientations of ϵ_1 recorded from both the medial and lateral surfaces of the lateral orbital wall during mastication and incision fall outside the range of values predicted by the tension hypothesis (cf. Figs. 12 and 13 with Fig. 4B,C). In sum, these data do not match the predictions of our formulation of the tension hypothesis, suggesting that the lateral orbital wall is not under tension during mastication and incision.

A model to explain patterns of bone strain in the circumorbital region of owl monkeys

The three hypotheses evaluated above posit what might be termed global or general loading regimes for the face and/or skull: they assume that the external forces acting on the face can be reduced to a single, most important bending or twisting moment that is of equal importance throughout the face. The facial-torsion hypothesis explicitly assumes that the patterns of stress and strain that this moment engenders can be predicted by modeling the skull as geometrically simple and structurally uniform (Greaves, 1985, 1995; Covey and Greaves, 1994). Overall, these hypotheses are not supported by the data reported here on bone strain in the face during mastication and incision. Perhaps the inadequacy of these hypotheses derives from inaccurate assumptions and inadequate knowledge of the biomechanics of the skull. Various masticatory muscle and bite forces act on the skull at several different locations, and our present knowledge of the

magnitude and orientation of these forces is poor. More importantly, the skull is a complex structure made up of bony members of varying shapes and orientations and composed of cortical bone of varying mechanical properties (cf. Dechow et al., 1993). Moreover, the bony elements are separated by various types of sutures, the biomechanical properties of which are only beginning to be explored (Herring and Mucci, 1991; Jaslow, 1990). Thus, modeling the entire skull as a simple beam or cylinder in most instances is simply too unrealistic (cf. Preuschoft et al., 1986).

We suggest that it is more productive to focus efforts on explaining local patterns of stress and strain in the skull by relating observed patterns of strain to external forces acting local to the area of interest. Only when we understand how individual areas of the skull (such as the postorbital bar, postorbital septum, or zygomatic arch) are behaving will a first step be made towards determining whether claims regarding more general loading patterns in the skull are realistic. For example, this approach has been applied profitably to the macaque mandible by first investigating patterns of stress and strain in the mandibular corpus (e.g., Hylander, 1981) and then the symphysis (Hylander, 1984). This approach has recently been extended to the zygomatic arch of macaques (Hylander and Johnson, submitted). Accordingly, a model relating observed patterns of bone strain in the lateral orbital wall (postorbital bar and septum) to the external forces acting in this area is presented below.

Review of patterns of bone strain in the lateral orbital wall. Although there is variability in patterns of bone strain orientation along the lateral orbital wall during mastication and incision, some generalizations are possible. ϵ_1 orientations on its lateral surface are oriented predominantly dorsoventrally. ϵ_1 orientations recorded from the medial surface are oriented predominantly rostrocaudally. On both medial and lateral surfaces, ϵ_1 orientations run in counterclockwise order from working side through incision to balancing side orientation (cf. Figs. 12–14). Of our six experiments, the only exception to this is experiment 10, in which this order is reversed. In all experiments, the orientations of ϵ_1 recorded from the medial surface of the postorbital septum are roughly orthogonal to those recorded from the lateral surface of the postorbital bar (cf. Fig. 14 with Figs. 12 and 13). This is particularly true when experiments 7 and 8 (Figs. 12, 13) are considered in conjunction with the septum experiments, 4 and 6 (Fig. 14).

Model relating external loads to patterns of strain orientation. If the lateral orbital wall is modeled as a thin curved plate, various combinations of compression, tension, and twisting can account for the in vivo strain data reported here. Dorsoventral compression of the plate, as might be expected on the working side during mastication or biting on the tooth row immediately adjacent to the plate's inferior root, will result in buckling (see Fig. 15, top). On the lateral surface of the plate ϵ_1 will be oriented along the dorsoventral axis of the plate, whereas ϵ_1 on the medial surface will be rostrocaudally oriented, orthogonal to the orientation of ϵ_1 on the lateral surface (Fig. 15). Under this loading regime, ϵ_1 is expected to be larger than ϵ_2 on the lateral surface, and ϵ_2 is expected to be larger than ϵ_1 on the medial surface.

When the plate is loaded in dorsoventral tension, as might be caused by contractions of masseter, the curved plate will become less curved, or unbent (see Fig. 15, middle). ϵ_1 on the lateral surface of the plate will be rostrocaudally oriented, whereas on the medial surface ϵ_1 will be oriented dorsoventrally along the plate, orthogonal to the orientation of ϵ_1 on the lateral surface (Fig. 15). ϵ_1 is expected to be larger than ϵ_2 on the medial surface, and ϵ_2 is expected to be larger than ϵ_1 on the lateral surface.

Twisting of the lateral orbital wall is possible due to the ventrocaudally directed component of the masseter muscle force acting on the lateral orbital wall at the anterior root of the zygomatic arch. The pattern of bone strain predicted for a thin plate twisted in this manner is shown in Figure 15 (bottom). ϵ_1 on the lateral surface of the plate would be oriented upwards to the left at 45° to the plate's long axis, whereas on the medial surface it will be oriented orthogonal to

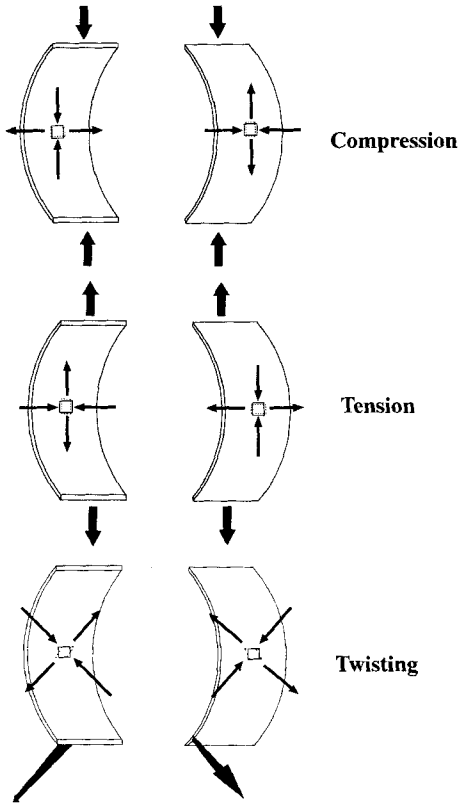

Fig. 15. Diagrams illustrating patterns of strain predicted in a curved plate subjected to dorsoventral compression (**top**), dorsoventral tension (**middle**), and twisting (**bottom**). Large arrows illustrate external forces producing the three loading regimes.

the orientation of ϵ_1 on the lateral surface. The predominant stress regime will be shear, and therefore the ratios of ϵ_1/ϵ_2 will be approximately equal.

Various combinations of these three loading regimes (buckling, unbending, and twisting) are possible. Moreover, if the loads causing the plate to be dorsoventrally compressed and dorsoventrally tensed are not aligned in exactly the same way, then the plate can be both buckled and unbent at the same time but in slightly different planes.

If the working side lateral orbital wall is modeled as a thin curved plate, then the in vivo strain orientation data suggest that it is being simultaneously buckled and possibly twisted (Figs. 12–14). The orientations of ϵ_1 recorded from the lateral surface of the lateral orbital wall are roughly orthogonal to those recorded from the medial surface, suggesting that the lateral orbital wall is being buckled. The orientations of ϵ_1 are counterclockwise or perpendicular to the toothrow, suggesting either that the septum is being buckled in a plane oblique to the tooth row or it is being twisted as well as buckled. The ϵ_1/ϵ_2 ratio data from experiments 6, 8, and 9 corroborate the hypothesis that the working side lateral orbital wall is being buckled: in experiment 6, ϵ_1/ϵ_2 ratios recorded from the medial surface of the balancing side septum are less than 1.0 (Table 12), and in experiments 8 and 9 ϵ_1/ϵ_2 ratios recorded from the lateral surface of the working side bar are greater than 1.0 (Tables 8, 10).

If the balancing side lateral orbital wall is modeled as a thin curved plate, then the in vivo strain orientation data from experiments 7, 8, and 9 suggest that it is being simultaneously buckled and twisted, with more twisting than on the working side. Buckling is suggested by the similarity with the working side strain orientations; greater twisting is suggested by the similarity with those expected for a pure twist (cf. Figure 15, bottom). This model does not explain why the ϵ_1 orientations recorded during experiment 10 run in clockwise rather than counterclockwise order from working side through incision to balancing side orientation. One possible explanation is that the gage in experiment 10 was located close enough to the anterior edge of the lateral orbital wall as to register edge effects.

The ϵ_1/ϵ_2 ratio data from these experiments do not consistently support the hypothesis that the balancing side lateral orbital wall is being buckled and twisted. ϵ_1/ϵ_2 ratios during buckling are expected to be greater than 1.0 on the lateral surface and less than 1.0 on the medial surface. ϵ_1/ϵ_2 ratios during twisting are expected to be close to 1.0 on both surfaces and perhaps closer to 1.0 than on the working side. The data recorded from the lateral surface of the balancing side postorbital bar during experiments 7 and 8 (Table 7a, 8a) and from the medial surface during experiment 4 (Table 12) support the twisting hypothesis, being very close to 1.0.

In experiment 6, the ϵ_1/ϵ_2 ratios recorded on the balancing side indicate more tension than compression on the medial surface, and in experiment 9 the ϵ_1/ϵ_2 ratios recorded on the balancing side indicate more compression than tension on the lateral surface. These ratios are the reverse of those recorded on the working side, suggesting that the balancing side lateral orbital wall is being unbent. However, pure unbending is difficult to reconcile with data on strain orientation, which suggest buckling and twisting. Data recorded during experiment 10 yielded ratios indicative of predominant compression on the lateral surface at all times (Table 11). Once again, these results may be attributable to edge effects.

In sum, if the lateral orbital wall is modeled as a thin curved plate, on the working side the predominant loading regime is buckling, probably due to the dorsally directed component of the bite force, with some twisting, due to caudoventrally directed components of the superficial masseter muscle force. On the balancing side, the strain orientation data and some of the ratio data suggest that the lateral orbital wall is also buckled and twisted but with twisting being of greater importance than on the working side. However, the data do not consistently support one hypothesized loading regime on the balancing side, so we hesitate to conclude definitively that these loading regimes predominate.

The model presented for the working side lateral orbital wall is supported by the in vitro data discussed above, which indicate that the working side lateral orbital wall experiences some degree of dorsoventral compression and buckling when the tooth row is loaded. In combination with the data gathered from the interorbital region, this suggests that the face is experiencing bending in the sagittal plane, with the working side lateral orbital wall being dorsoventrally compressed. The degree of dorsoventral compression is greatest when the bite point is immediately below the inferior root of the ipsilateral lateral orbital wall, with the degree of twisting increasing as the bite point moves away from the inferior root of the lateral orbital wall.

Data gathered from simultaneous EMG studies indicate that the working side masseter is, on average, about 1.3 times more active than the balancing side during powerful mastication, so why are the effects of masseter forces only hypothesized to be reflected in patterns of bone strain in the balancing side lateral orbital wall? The model proposed here suggests that buckling of the working side lateral orbital wall occurs only when the animal is chewing on the molars immediately adjacent to the inferior root of the ipsilateral postorbital bar, because only in these circumstances will the dorsally directed component of the bite force be sufficient to swamp the effects of force from the working side masseter. Support for this hypothesis comes from the observation that the pattern of strain orientations seen on the working side are only seen during mastication or unilateral *molar* biting ipsilateral to the strain gage. Ipsilateral premolar biting and incisor biting are accompanied by patterns of bone strain orientation similar to those seen during mastication and molar biting contralateral to the strain gage.

Strain magnitudes: How much strain is too much strain?

The three hypotheses tested above all claim that the postorbital septum evolved in order to maintain the structural integrity of the facial skeleton. These hypotheses were evaluated in two ways. First, bone-strain levels in the circumorbital region were analyzed in vitro in an owl monkey skull with and without intact postorbital septa. Second, bone-strain magnitudes in the owl monkey circumorbital region were measured in vivo.

In vitro strain magnitudes: The effects of loss of the postorbital septum. In vitro incisor loading appears to bend the face in the sagittal plane, buckling the lateral orbital margins, both before and after cutting the postorbital septa. Strain magnitudes in the circumorbital region are lower after the septa were cut than before, suggesting that the postorbital septum does not function to reduce bone strain magnitudes in the circumorbital region during loading of the incisors.

Unilateral loading of the tooth row in the intact skull also appears to bend the face in the sagittal plane, buckling the lateral orbital margins. Because the face is loaded to one side of the midline, a twist must also occur, but the strains appear to indicate that the most important loading regime is sagittal bending. Once the septa are cut, however, strain orientations suggest that the palate bends or "seesaws" over to the working side relative to the braincase, resulting in buckling of the working side lateral orbital wall and unbending of the balancing side lateral orbital wall (Fig. 10). The face is probably also bent in the sagittal plane, resulting in rostrocaudal compression of the interorbital region. When torsion of the face is induced by loading the premolars, strain magnitudes in the interorbital region increase somewhat after cutting the septa, but strain magnitudes in the lateral orbital walls are generally lower. When torsion is induced by loading the molars, strain magnitudes in the interorbital region and lateral orbital wall increase when the septa are cut. Thus, the postorbital septum appears to counter the tendency for the palate to seesaw on the braincase when loads are applied to the molars.

In vitro strains recorded from the working side lateral orbital wall resemble in vivo strains recorded from the working side lateral orbital wall. In both cases the lateral orbital wall appears to be buckled. This resemblance allows us to apply the results of the in vitro experiment to answering the question: How might the absence of the postorbital septa affect in vivo strain magnitudes along the working side postorbital bars of owl monkeys?

In vitro, cutting the septa results in an increase in ϵ_1 magnitudes in the working side lateral orbital wall of 40% on the lateral surface and 10% on the medial surface when the molars are loaded. ϵ_2 magnitudes in the working side lateral orbital wall increase by 44% on the lateral surface but do not change significantly on the medial surface at this time. If in vivo bone strain magnitudes in the owl monkey working side postorbital bar increased by these amounts, they would exceed those recorded from the mandible. It appears, therefore, that the septum does reduce strain magnitudes in the postorbital bar but only during loading of the ipsilateral postcanine tooth row.

In vivo strain magnitudes. To address the question of whether the owl monkey circumorbital region experiences high or low levels of strain, the strain data from this region are compared with data from elsewhere in the masticatory apparatus (Hylander et al., 1991). If bone strain magnitudes recorded from the circumorbital region are similar to or higher than the highest magnitudes and ranges recorded elsewhere, this suggests that the circumorbital bones have a comparatively small safety factor to failure. In the context of the in vitro results reported above—under certain loading conditions, destroying the structural integrity of the postorbital septum results in increased bone strain magnitudes—relatively high bone-strain magnitudes and ranges in the circumorbital region might suggest that the absence of a postorbital septum could compromise the structural integrity of the skull.

With this rationale in mind, strain magnitudes recorded from the working side postorbital bar during incision and mastication of hard foods are compared below with those recorded simultaneously from the working side mandible (experiments 9 and 10). Comparisons of working side mastication values are of interest because it is on the working side that the highest strains are normally found and it is during mastication that the effects of high frequency cyclical loading are most liable to accumulate. Comparison of incision values is also of interest because incision of hard food objects is often accompanied by high bone-strain magnitudes. Comparisons of postorbital bar bone-strain magnitudes with those recorded from the mandible are appropriate because experiments with macaques have revealed the mandible to be usually the most highly loaded bone during mastication (Hylander et al., 1991), incurring principal strains up to 2,000 $\mu\epsilon$ during isometric biting.

During experiment 10, all bone strain magnitudes (i.e., ϵ_1, ϵ_2, and γ-max means and

maxima) recorded from the postorbital bar were lower than those recorded simultaneously from the mandible (Table 11). Moreover, during experiment 9, ϵ_2 means and maxima recorded from the postorbital bar were always lower than those recorded simultaneously from the mandible. However, during experiment 9, some ϵ_1 values recorded from the postorbital bar were higher than those recorded simultaneously from the mandible (96 mastication power strokes out of a total of 411 [23%]). The maximum ϵ_1 recorded from the working side postorbital bar was higher than that recorded from the working side mandibular corpus during mastication of both hard prune and gummy bears, and the mean and maximum ϵ_1 recorded from the working side postorbital bar were higher than those recorded from the working side mandibular corpus during mastication of hard apricot (Table 10). And, because γ-max values are calculated as ϵ_1-ϵ_2, some of the γ-max values recorded from the postorbital bar were also higher than those recorded from the mandibular corpus (20 out of 519 power strokes [3.9%], with the greatest difference between the two areas being 126 $\mu\epsilon$) (Table 10). Thus, during experiment 9, γ-max and ϵ_1 magnitudes recorded from the postorbital bar during mastication did occasionally exceed those recorded from the mandible. Overall, however, the strains in the mandibular corpus are generally higher than those recorded in the postorbital bar—the mean ratios indicate that the working side mandibular corpus has generally higher γ-max values than the working side postorbital bar during incision and mastication (Table 10). These results suggest to us that the owl monkey lateral orbital wall generally has a somewhat greater safety factor to yield than the mandibular corpus.

CONCLUSIONS

The in vitro and in vivo data presented above support the possibility that, in owl monkeys, the presence of the postorbital septum improves the structural integrity of the postorbital bar by lowering bone strain magnitudes during mastication. However, in vivo strain magnitudes in the septum are only occasionally higher than in the mandibular corpus, and then only slightly. Furthermore, removal of the septum in vitro is accompanied by significant decreases in strain magnitudes throughout the face during incisor loading. Consequently, we are unable to conclude unequivocally that the septum in these extant anthropoids functions to improve the structural integrity of the skull.

Greaves (1985) suggested that the postorbital septum evolved from a postorbital bar because the highly approximated orbits of anthropoids reduce the ability of the face to resist twisting moments during mastication and that the postorbital septum is particularly apt for resisting this twisting because it is situated well away from the twisting axis of neutrality. However, the in vitro data presented here suggest that unilateral loading of the tooth row does not result in detectable twisting of the face on the braincase, even in the absence of the septum. Furthermore, the in vivo data indicate that twisting of the face on the braincase is not an important loading regime during mastication, at least in this extant anthropoid. Rather, it appears that the face is mainly bent in the sagittal plane during mastication and incision so that the working side lateral orbital wall is dorsoventrally compressed and buckled at this time.

If the predominant working side loading regime in the lineage that evolved the septum was the same as that observed in these owl monkeys (i.e., dorsoventral compression and buckling), it is unlikely that the septum evolved to resist masticatory loads in the circumorbital region. A postorbital bar, not a postorbital septum, provides the best arrangement of material for resisting bucking, as readers can easily demonstrate for themselves. When a sheet of paper is held so as to form a gentle curve—much like a postorbital septum—it is easily buckled by pushing the ends together. However, when the sheet is rolled into a tube—like a postorbital bar—and the tube compressed along its long axis by pushing the ends of the tube towards each other, the same sheet of paper has a vastly improved ability to resist axial compression and buckling. Similarly, a postorbital bar is much better at resisting dorsoventral com-

pression and buckling than an equivalent amount of bone mass in the form of a postorbital septum, and, if buckling was the predominent working side loading regime when the septum evolved, resistance of masticatory forces is unlikely to have been its original function.

Thus, although the postorbital septum appears to provide structural reinforcement of the face in some extant anthropoids, it seems unlikely that this was its original function. Rather, the septum probably arose to insulate the orbital contents against movements in the temporal fossa in the context of increasing convergence and frontation of the orbital margins in the small-bodied diurnal haplorhine stem lineage (Ross, 1995; in press). Once present, the septum may have enabled the postorbital bar to be reduced in robusticity, as it is in small extant anthropoids, but subsequent increases in body size appear to have been accompanied by increases in the robusticity of the postorbital bar, while the septum remained relatively thin (e.g., large-bodied catarrhines and platyrrhines). At present, however, there is no strong evidence to support the hypothesis that the septum in extant anthropoids is important for maintaining the structural integrity of the skull.

ACKNOWLEDGMENTS

This study would have been impossible without the loan of two owl monkeys from Batelle Labs, kindly facilitated by Dr. Richard Weller, and the loan of an owl monkey cadaver from the Smithsonian Institution, courtesy of Dr. Richard Thorington. We would like to thank the staff at the Duke University Vivarium, particularly Dr. Rick Rahija, for help during this study. X. Chen, D. Daegling, B. Demes, D. Lieberman, and B. Richmond provided useful comments on the manuscript. Dave Daegling kindly assisted with the in vitro experiment. This research was supported by grants from NSF (BNS-91-00523) to W.L.H. and C.F.R. and NIH Merit Award (DE04531) to W.L.H.

LITERATURE CITED

Cachel S (1979) A functional analysis of the primate masticatory system and the origin of the anthropoid post-orbital septum. Am. J. Phys. Anthropol. *50*:1–18.

Cartmill M (1980) Morphology, function and evolution of the anthropoid postorbital septum. In RL Ciochon and AB Chiarelli (eds.): Evolutionary Biology of the New World Monkeys and Continental Drift. New York: Plenum, pp. 243–274.

Connolly R, and Quimby FW (1978) Acepromazine-ketamine anesthesia in the rhesus monkey (*Macaca mulatta*). Lab. Anim. Sci. *28*:72–74.

Covey DS, and Greaves WS (1994) Jaw dimensions and torsion resistance during canine biting in the Carnivora. Can. J. Zool. *72*:1055–1060.

Dally JW, and Riley WF (1965) Experimental Stress Analysis. New York: McGraw-Hill.

Dechow P, Nail GA, Schwartz-Dabney CL, and Ashman RB (1993) Elastic properties of human supraorbital and mandibular bone. Am. J. Phys. Anthropol. *90*: 291–306.

Greaves WS (1985) The mammalian postorbital bar as a torsion-resisting helical strut. J. Zool. Soc. (Lond.) *207*:125–136.

Greaves WS (1995) Functional predictions from theoretical models of the skull and jaws in reptiles and mammals. In JJ Thomason (ed.): Functional Morphology in Vertebrate Paleontology. New York: Cambridge University Press, pp. 99–115.

Herring SW, and Mucci RJ (1991) In vivo strain in cranial sutures: The zygomatic arch. J. Morphol. *207*:225–239.

Hylander WL (1981) Patterns of stress and strain in the macaque mandible. In DS Carlson (ed.): Craniofacial Biology. Monograph 10. Craniofacial Growth Series. Center for Human Growth and Development. Ann Arbor: University of Michigan, pp. 1–37.

Hylander WL (1984) Stress and strain in the mandibular symphysis of primates: A test of competing hypotheses. Am. J. Phys. Anthropol. *64*:1–46.

Hylander WL, and Johnson KR (submitted) In vivo bone strain patterns in the zygomatic arch of macaques and the significance of these patterns for functional interpretations of craniofacial form. Am. J. Phys. Anthropol.

Hylander WL, Picq PG, and Johnson KR (1991) Masticatory-stress hypotheses and the supraorbital region of primates. Am. J. Phys. Anthropol. *86*:1–36.

Hylander WL, Johnson KR, and Crompton AW (1992) Muscle force recruitment and biomechanical modeling: An analysis of masseter muscle function during mastication in *Macaca fascicularis*. Am. J. Phys. Anthropol. *88*:365–387.

Jaslow CR (1990) Mechanical properties of cranial sutures. J. Biomech. *23*:313–321.

Preuschoft H, Demes B, Meyer M, and Bar HF (1986) The biomechanical principles realised in the upper jaw of long-snouted primates. In JG Else and PC Lee (eds.): Primate Evolution. Cambridge: Cambridge University Press, pp. 249–264.

Rosenberger AL (1986) Platyrrhines, catarrhines and the anthropoid transition. In BA Wood, L Martin, and

P Andrews (eds.): Major Topics in Primate and Human Evolution. Cambridge: Cambridge University Press, pp. 66–88.

Ross CF (1993) The functions of the postorbital septum and anthropoid origins. Ph.D. Dissertation, Duke University. Ann Arbor: UMI Dissertation Services.

Ross CF (1995) Muscular and osseous anatomy of the primate anterior temporal fossa and the functions of the postorbital septum. Am. J. Phys. Anthropol. *98*:275–306.

Ross CF (1996) An adaptive explanation for the origins of the Anthropoidea (Primates). Am. J. Primatol. (in press).